Effect of Surface Modes on the Six-Dimensional Molecule-Surface Scattering Dynamics of H-2-Cu(100) and D-2-Cu(111) Systems

ARTICLE *in* THE JOURNAL OF PHYSICAL CHEMISTRY A · JUNE 2011

Impact Factor: 2.69 · DOI: 10.1021/jp201524x · Source: PubMed

THE JOURNAL OF PHYSICAL CHEMISTRY A

ARTICLE

pubs.acs.org/JPCA

Effect of Surface Modes on the Six-Dimensional Molecule−Surface Scattering Dynamics of H_2−Cu(100) and D_2−Cu(111) Systems

Tapas Sahoo,[†] Subhankar Sardar,[†] Padmabati Mondal,[†] Biplab Sarkar,[‡] and Satrajit Adhikari[†,*]

[†]Department of Physical Chemistry, Indian Association for the Cultivation of Science, Jadavpur, Kolkata 700 032, india

[‡]Department of Chemistry, North-Eastern Hill University, Shillong 793 022, india

ABSTRACT: We include the phonon modes originating from the three layers of Cu(100)/Cu(111) surface atoms on the dynamics of molecular [$H_2(v,j)$/$D_2(v,j)$] degrees of freedom (DOFs) through a mean field approach, where the surface temperature is incorporated into the effective Hamiltonian (potential) either by considering Boltzmann probability (BP) or by including the Bose−Einstein probability (BEP) factor for the initial state distribution of the surface modes. The formulation of effective potential has been carried out by invoking the expression of transition probabilities for phonon modes known from the "stochastic" treatment of linearly forced harmonic oscillator (LFHO). We perform four-dimensional (4D⊗2D) as well as six-dimensional (6D) quantum dynamics on a parametrically time and temperature-dependent effective Hamiltonian to calculate elastic/inelastic scattering cross-section of the scattered molecule for the H_2 (v,j)−Cu(100) system, and dissociative chemisorption−physisorption for both $H_2(v,j)$−Cu(100) and $D_2(v,j)$−Cu(111) systems. Calculated sticking probabilities by either 4D⊗2D or 6D quantum dynamics on an effective potential constructed by using BP factor for the initial state distribution of the phonon modes could not show any surface temperature dependence. In the BEP case, (a) both 4D⊗2D and 6D quantum dynamics demonstrate that the phonon modes of the Cu(100) surface affect the state-to-state transition probabilities of the scattered H_2 molecule substantially, and (b) the sticking probabilities due to the collision of H_2 on Cu(100) and D_2 on Cu(111) surfaces show noticeable and substantial change, respectively, as function of surface temperature only when the quantum dynamics of all six molecular DOFs are treated in a fully correlated manner (6D).

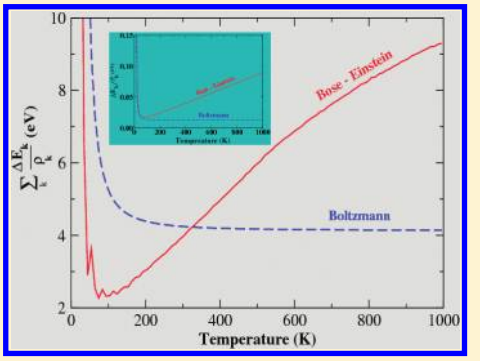

I. INTRODUCTION

The scattering and dissociative chemisorption of molecules on metal surfaces have been intensively explored during the last few decades.[1−16] The advancement of experimental techniques,[2−5] especially associative desorption[2] and molecular beam[3,4] experiments have contributed significantly to refine the theoretical developments on the computation of the potential energy surfaces (PESs)[17−24] and the formulation of molecular dynamics methodologies.[25−40] The adsorption of H_2 on metal surfaces has been investigated as the paradigm of gas−surface reaction dynamics, where the dissociation of H_2 on copper is a benchmark system for activated surface reaction dynamics for both experimental and theoretical studies. The first 6D quantum dynamical calculations of nonactivated dissociative adsorption and associative desorption on the H_2/Pd(100) system was performed by Gross et al.[34] using the PES obtained from density functional theory (DFT). The reaction probabilities as functions of initial translational energy of the diatom in case of H_2−Cu(1nn) collision are calculated by 6D quantum dynamics[34−43] with a rigid surface (RS) and compared with the fitted profiles[6] of *associative desorption*[2] *as well as molecular beam*[3] experimental results. On the other hand, Dai et al.[35] constructed the PES for H_2 on Cu(111) surface utilizing previously calculated ab initio data[17] and reported their preliminary 6D quantum dynamical results for activated dissociative adsorption, and such calculations were almost simultaneously performed with the work of Kroes et al.[36] Watts et al.[4] depicted the theoretically calculated rovibrationally resolved transition probabilities for the $H_2(v=1,j=1)$−Cu(100) system with experimentally measured quantities. Experimentally, they have used the molecular beam technique with stimulated Raman pumping to overpopulate (v = 1, j = 1) the incident beam, whereas the resonance enhanced multiphoton ionization technique is applied to detect the scattered $H_2(v'=1,j')$ at 500 K. The temperature-dependent sticking probabilities for D_2 on the Cu(111) surface are also known from the analysis[7] of experimentally measured adsorption data,[9] and such reaction probabilities show slight broadening at low and high initial kinetic energies (KEs) over the temperature range 120−1000 K. Díaz et al.[37] implemented specific reaction parameter (SRP) approach on DFT to obtain the molecule−surface interaction potential and performed the 6D quantum dynamics for various initial rovibrational states of H_2 impinging on Cu(111) surface, and reproduced the results fitted from molecular beam experiment on the dissociative adsorption probability as a function of incidence energy.

Received: February 15, 2011
Revised: April 11, 2011
Published: May 05, 2011

While modeling the molecule−surface scattering processes, there are limited attempts to include two important phenomena, namely, *surface mode vibration* and *electron hole−pair excitation* either in full or even in reduced dimensional quantum calculations. The dynamical calculations including the surface mode(s) have been performed on the basis of two types of broad approaches, where in one case, the Hamiltonian has been constructed by incorporating a single oscillator[28−30,44−46] (harmonic/Morse) and in another case, many oscillators[32,33,47−50] (harmonic) representing a particular metal surface [Cu(1*nn*)] with its specific plane [(1*nn*), *n* = 0, 1] are included. While solving the time-dependent Schrödinger equation (TDSE), the single oscillator based approaches obviously can consider multiple configurations to take into account the interaction between the molecular DOFs and the surface oscillator accurately. On the other hand, the effect of surface oscillators on the molecule surface scattering has so far been explored by considering a mean-field approach, i.e., a product between the molecular wave function and the wave function for the oscillators.

Hand and Harris[44] as well as Dohle and Saalfrank[46] considered a single ordinary surface oscillator (SO) and a modified surface oscillator (MSO), respectively, with a microscopically motivated molecule−surface coupling to investigate the effect of the motion of surface atoms on the dissociation dynamics of H_2 on Cu(111) surface. In SO calculations, the relevant Hamiltonian is constituted with three DOFs, namely, the normal distance of the molecular center of mass (COM) from the surface plane (Z), the bond distance between the two nuclei (r), and the simple oscillator (d) for the surface. Dohle and Saalfrank[46] have compared their MSO results calculated at different surface temperatures with the RS profiles and observed a small shift of the sticking probability curve toward the threshold energy with a slight broadening; i.e., as the surface temperature goes up, the reaction probability increases and decreases at low and high collision energy, respectively. It is important to note that the reaction probabilities calculated on the basis of the SO approaches show the reverse feature in contrast to the sticking probabilities obtained by employing MSO based models; i.e., the former cases depict higher energy shift of the reaction probabilities compared to the lower energy shift in the case of later ones. Holloway et al.[28] followed the similar approach of Hand and Harris[44] and treated the substrate motion as a single Einstein oscillator with the mass of one Cu atom and the Debye frequency (ω_D) of the surface. Their calculations were performed with a Hamiltonian by including four (4) molecular DOFs (Z, r, θ and ϕ) and one surface oscillator coordinate (d). Such lower dimensional models with a single surface mode for the H_2−Cu(111) system show (a) the molecule loses energy to the repulsive wall of the PES as the surface recoils, where the recoil of the lattice atoms is small because of the large mass difference between the molecule and the surface atoms and (b) the thermal motion of the surface atoms increases leading to a Doppler downshift of activation barriers for dissociation and transition probabilities, if there is no trapping before collision. The effect of lattice motion and the role of lattice reconstruction for the dissociation of methane on Ni(111) surface at various temperatures have been investigated[29−31] by carrying out the dynamics on a 4D PES, $V(Z,r,\theta,Q)$, where the activation energy for the reaction varies with the surface oscillator (Morse) coordinate, Q. Tiwari et al.[31] have implemented the so-called sudden approximation approach by introducing a Boltzmann distribution of lattice positions, Q. For each fixed value of Q, the calculation has been performed by treating Z, r, θ, and ϕ quantum mechanically, and finally, those results are averaged. Such calculated results suggested that sudden treatment of the lattice could be reasonably valid. On the contrary, in our approach, because the average over the lattice coordinates (Q_k) has been carried out (due to the introduction of mean-field approximation) by all possible initial configurations [see the summation over the initial states, n_k^0, in Φ_0^p and thereby, in eq A1] of the phonon modes arising from the Boltzmann or Bose−Einstein distribution, the implementation of sudden approximation is not possible. If one can formulate a multiconfiguration Hartree-based approach, the possibility of introducing sudden approximation remains but the infinitely large number of configurations arising due to Boltzmann or Bose−Einstein distribution of the phonon states to introduce surface temperature accurately may lead to a computationally intractable approach.

The single oscillator based treatments are more phenomenological approaches to investigate the effect of surface temperature on the molecule−surface scattering processes rather than a quantitative theory to incorporate the details of a particular metal surface [Cu(1*nn*)] and its specific plane [(1*nn*), *n* = 0, 1]. In the case of quantitative treatment, one can consider the coupling between the surface modes and the diatomic DOFs to be strong enough to warrant a fully correlated description, where a time-dependent superposition of all possible configurations of the surface modes (arising due to the Boltzmann or Bose−Einstein distribution of the phonon states) and the states described by the molecular DOFs are taken into account. That essentially leads to a multiconfiguration time-dependent Hartree (MCTDH) approach. Considering the present problem, such an approach will require an infinitely large number of configurations to represent the surface temperature accurately and, thereby, become computationally prohibitive. On the contrary, it may be possible to make progress by assuming a weak correlation between molecular DOFs and surface modes, and incorporating the effects of surface modes into the molecular DOFs through a mean-field approach. This approach could be formulated by considering a Hartree type product of surface and molecular wave functions, where the surface wave function may be constructed possibly by including all configurations of the phonon states accessible at the given temperature. Because the energy transfer turns out to be sufficiently small compared to the highest initial kinetic energy of the diatom within the range of surface temperature of our investigation, a posteriori justification for assuming weak correlation between molecular DOFs and surface modes can be provided. So, a mean-field approach, where the surface wave function includes all possible configurations of the phonon states will be a pragmatic one for quantitative handling of the effects of phonon modes in a molecule−surface scattering.

The dissociative chemisorption and scattering cross-section of H_2/Cu(111) system were investigated by employing a mean-field approach,[49] where the four molecular DOFs (Z, r, θ, and ϕ) are considered strongly coupled with each other but weakly interact with the other molecular coordinates (X and Y) and the surface modes. Such treatments are involved[32,33,49] with the second quantization formulation of molecular dynamics[47,48] including BP factor for initial state distribution of the phonon modes. In the present formulation,[50] (a) the time evolution of the phonon modes has access to all possible configurations arising due to the phonon states of the various modes and (b) the effective potential, which enters into the molecular Hamiltonian, has been derived by taking into account the average over the molecule−surface interaction potential by all those configurations due to the initial state

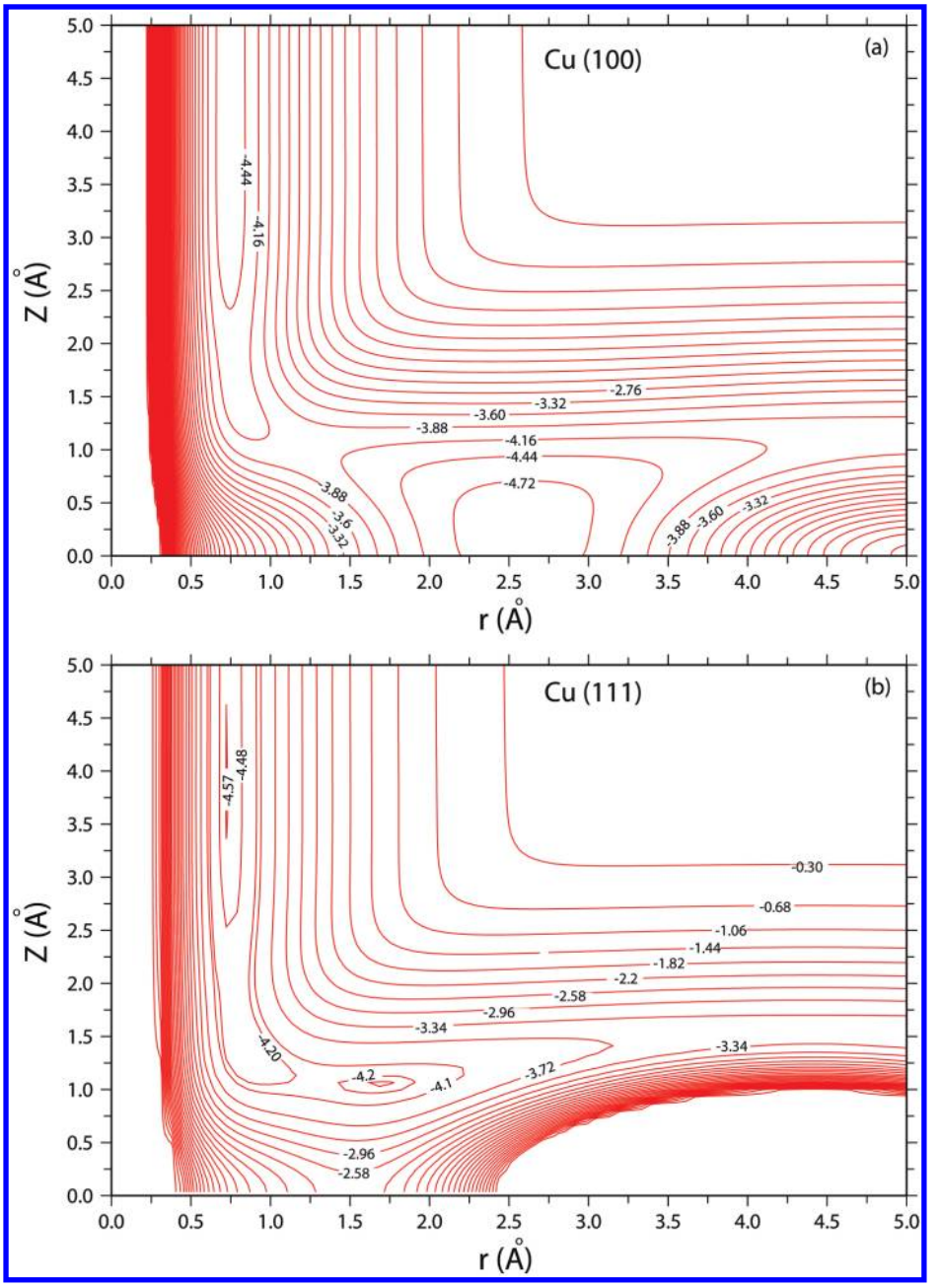

Figure 1. Contour plot of EDIM-fit ground adiabatic PES for H_2 and D_2 interacting on the bridge site and dissociating to the hollow site of the (a) Cu(100) and (b) Cu(111) surface, respectively.

distribution either by including BP or by incorporating BEP factor [see the summation over the initial states, n_k^0, in Φ_0^p and thereby, in eq A1]. Indeed, the analytic form of the effective potential, which appears due to the initial distribution of the phonon states by BP factor clearly shows that it fails to capture the effect of surface temperature on the molecular DOFs.

In this article, we perform the reaction dynamics on the ground adiabatic (Born−Oppenheimer (BO)) surface constructed by embedded diatomics in molecules (EDIM) approach [see section II] and explore the effect of phonon modes on the dissociative chemisorption and scattering processes. For this purpose, it is necessary to evaluate the derivative(s) of the interaction potential to include the phonon forcing, where a weak interaction is assumed between the molecular DOFs and the phonon modes to formulate the time and temperature-dependent effective Hamiltonian [see section IIIA] for molecule−surface scattering. Finally, we present the corresponding quantum dynamical equations of motion [see sections IVA and IVB] and demonstrate the workability of time-dependent discrete variable representation (TDDVR) method[55−66] for scattering processes [see section IVC and first paragraph of section V]. In the results and discussion section [see section V], we intend to find the answers of the three following major questions: (a) Can the mean-field approximation between molecular DOFs and the phonon modes incorporate, if at all, the effect of surface temperature on the scattering dynamics of the molecular DOFs? (b) Which one of the effective potentials either derived by Boltzmann or formulated by BEP factor can demonstrate the effect of surface temperature on the

Table 1. Barrier Heights (E_b) and Their Locations (r_b and Z_b) for H_2 Dissociating with Its Molecular Axis Kept Parallel to the Cu(100) Surface[a]

impact site	dissociation to	E_b (eV)	r_b (Å)	Z_b (Å)
bridge	hollow	0.50 (0.48)	1.22 (1.23)	1.05 (1.05)
hollow	bridge	0.55 (0.63)	1.20 (1.00)	1.17 (1.14)
top	bridge	1.10 (0.72)	1.35 (1.43)	1.45 (1.40)
bridge	top	1.23 (1.37)	1.88 (2.09)	1.52 (1.52)

[a] The numbers in the parentheses are the results of Wiesenekker et al.[21]

Table 2. Barrier Heights (E_b) and Their Locations (r_b and Z_b) for D_2 Dissociating with Its Molecular Axis Kept Parallel to the Cu(100) Surface[a]

impact site	dissociation to	E_b (eV)	r_b (Å)	Z_b (Å)
bridge	hollow	0.38 (0.63)	1.08 (1.03)	1.30 (1.17)
top	bridge	0.80 (0.89)	1.32 (1.40)	1.48 (1.39)

[a] The numbers in the parentheses are the results of Díaz et al.[37]

molecular DOFs? (c) To what extent are the molecular coordinates, X and Y, important to depict the temperature dependence on the calculated sticking probabilities, i.e., 4D⊗2D[50] verses 6D calculations, to show the importance of X and Y coordinates to incorporate the effect of phonon modes on the molecule−surface scattering?

II. EDIM POTENTIAL FOR H_2/D_2−CU(1NN) INTERACTION

Though various levels of ab initio calculations have been carried out on the H_2−Cu(1nn) system, the quality of the surfaces is still debated due to the "necessary" approximation involved in those calculations. As for the barrier of dissociative chemisorption from bridge to hollow site (bth) for H_2/Cu(100) system, the experiment[3] inferred the value should be 0.5−0.7 eV but ab initio calculation with local density approximation (LDA)[18] for slab predicted about 0.3 and 1 eV with SCF/CI calculation[19] for cluster. Those calculated potential energies obtained from LDA or SCF/CI method are not good quality to describe the H_2/Cu(100) system. On the other hand, White et al.[20] performed a generalized gradient approximation (GGA) calculation involving Perdew and Wang[51] modifications on a too small size *surface unit cell* and evaluated the bth barrier height ∼0.93 eV. Still these potential parameters and corresponding PESs are not sufficiently accurate to be used in further dynamical calculation. Wiesenekker et al.[21] calculated the PESs for slab by using a different GGA with Becke[52] and Perdew[53] corrections and found the bth barrier height ∼0.48 eV, which is qualitatively correct to the experimental data. Kratzer et al.[22] used the plane wave basis pseudopotential and employed Perdew−Wang GGA approach to calculate the PESs and obtained the barrier height at 0.6 eV. The *most recent and accurate* PESs with the barrier height ∼0.63 eV for the H_2−Cu(111) system are obtained from SRP-DFT[37] calculation.

With this background information on ab initio data, we construct an analytical potential energy surface by the using EDIM method as proposed by Truong et al.[23] Because the purpose of our present article is to explore how the phonon modes of the low index Cu surface affect the sticking probabilities of the incoming diatom and the state-to-state transition probabilities of the scattered molecule, we developed the EDIM potential by using DFT-GGA data[21] and compared the potential values with the available results.[17,21,37]

H_2−Cu(100): The barrier heights and their locations on the EDIM fit are summarized in Table 1. In the entrance channel (for large values of Z), the interaction of the H_2 molecule with the Cu(100) surface is negligible. The GGA dissociation energy (D_e) of the free H_2 molecule is −4.83 eV, while the binding energy (D_b) of a H atom is −2.7 eV in the hollow site. This dissociation process is exothermic by $2 \times D_b - D_e = 0.56$ eV. Similarly, dissociation into bridge site is slightly exothermic by 0.20 eV, whereas dissociation on the top site is endothermic by 1.65 eV. Figure 1a *shows the PES for dissociation from a bth site with lowest barrier height ∼0.50 eV and it is located in the exit channel at r_b = 1.22 Å and Z_b = 1.05 Å*. The same figure depicts that the H atoms are adsorbed on the hollow site with a minimum value of Z (≈0.5 Å) and large value of r. On the other hand, the PES for dissociation from a top to it is neighboring bridge (ttb) site differs markedly from the PES for dissociation from the bth site [Figure 1a]. Table 1 also shows the ttb barrier height, E_b = 1.10 eV and its location at r_b = 1.35 Å and Z_b = 1.45 Å. The barrier height (0.55 eV) of the EDIM PES for dissociation from a hollow to bridge site is comparable (E_b = 0.63 eV) with the parameter of Wiesenekker et al.,[21] whereas our calculated E_b for ttb overestimates noticeably.

D_2−Cu(111): Table 2 presents the barrier heights and their locations on the EDIM fit in case of D_2−Cu(111) system. Figure 1b shows the PES for dissociation from a bth site with lowest barrier height 0.38 eV and it is located in the exit channel at r_b = 1.08 Å and Z_b = 1.30 Å, where the barrier height for ttb dissociation geometry is 0.80 eV and the corresponding barrier geometry is r_b = 1.32 Å, Z_b = 1.48 Å. The minimum barrier height in the case of bth with EDIM fit depicts a good agreement with the earlier results of Hammer et al.[17] estimated in the range 0.46−0.52 eV, but Díaz et al.[37] have calculated the bth E_b = 0.63 eV using a SRP approach to DFT. On the other hand, our calculated E_b data for ttb site shows reasonable agreement with the SRP-DFT data (0.89 eV).

IIIA. THEORETICAL DEVELOPMENT EMPLOYING THE MEAN-FIELD APPROACH

Because theoretically calculated reaction probabilities[46] using MSO model for H_2 on Cu(111) surface within the temperature range 0−1000 K and the analysis of experimentally measured sticking probabilities[7] for D_2 on Cu(111) surface over the temperature range 120−1000 K show *only slight broadening*, particularly, at low and high initial KEs, a mean-field approach with a product wave function built up from wave functions associated with surface and molecular DOFs could be appropriate. The surface wave function may be defined by only one or few or all possible configuration(s) of the phonon states. The inclusion of only one or few configuration(s) will represent the surface at a given temperature very crudely, and thereby, the construction of the surface wave function with all possible configurations of the phonon states is a necessity to mimic the surface temperature accurately. On the contrary, the assumption of weak correlation between molecular DOFs and surface modes may fail to produce the required effects of the surface on the molecular DOFs at a given temperature as much as it should. As the interaction between the molecular DOFs and surface modes is weak enough, which could be explored in this article by calculating the energy transferred from solid to the diatom and vice versa, the assumption regarding

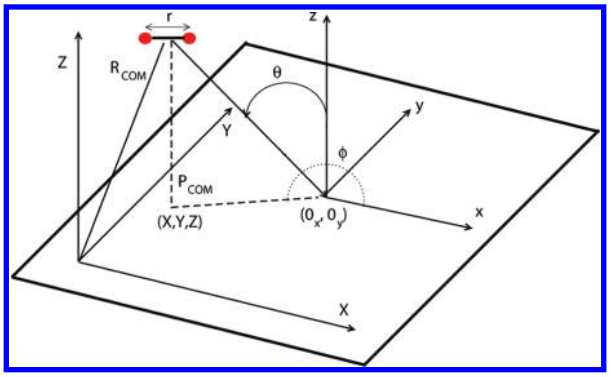

Figure 2. Molecular (H_2/D_2) coordinates on a metal surface.

the weak correlation (that is exploited to arrive at the mean-field description) may be reasonably valid. Moreover, as the copper crystal is modeled by 133 atoms placed in 3 layers [$(1nn)$ plane] in our present calculation (to reach the required convergence) and a fully correlated dynamics due to the inclusion of all possible configurations of the phonon states and the molecular DOFs is computationally intractable, the coupling between the molecule and the 393 phonon modes originating from the surface atoms ($N = 133$) is incorporated within the mean-field approximation on the wave function as given below:

$$\Psi(x,y,z,X,Y,Z,t)\cdot\Phi(\{Q_k\},t) \qquad (1)$$

where the time evolution of the phonon modes (Q_k's) has been allowed to access all possible configurations arising due to their various quantum states.

Such product-type wave function [eq 1] brings the following form of time and temperature-dependent effective Hamiltonian ($H(\{\chi_k\},t,T_s),\{\chi_k\} \equiv x,y,z,X,Y,Z$) to govern the motion of the incoming molecule (6D) with respect to surface atoms:

$$-\frac{\hbar^2}{2\mu}\left(\frac{\partial^2}{\partial x^2}+\frac{\partial^2}{\partial y^2}+\frac{\partial^2}{\partial z^2}\right)-\frac{\hbar^2}{2M}\left(\frac{\partial^2}{\partial X^2}+\frac{\partial^2}{\partial Y^2}+\frac{\partial^2}{\partial Z^2}\right)$$
$$+V_0(x,y,z,X,Y,Z)+V_{\text{eff}}(x,y,z,X,Y,Z,t,T_s) \qquad (2)$$

where μ and M are the reduced and total mass of the diatom, respectively. The Cartesian coordinates x, y, z represent the molecular vector $\vec{r}(r,\theta,\phi)$ and X, Y, Z are the COM position of the molecule with respect to the Cu surface such that the top layer of the Cu atoms corresponds to $Z = 0$.

Because the dynamical calculation on such effective Hamiltonian involved with six molecular DOFs (x, y, z, X, Y, and Z) is computationally very much demanding, we also examine the well-known approximation, namely, the coordinates, x, y, z, and Z are strongly coupled (4D⊗2D) with each other but weakly interact with the COM coordinates, X and Y, and explore the importance of phonon modes on the scattering dynamics considering the product-type wave function[50] among the molecular coordinates as given below:

$$\Psi(x,y,z,X,Y,Z,t) = \Psi_1(x,y,z,Z,t)\cdot\Psi_2(X,Y,t) \qquad (3)$$

When the dynamics of the molecule (x, y, z) with respect to the surface (X, Y, Z) is considered as strongly coupled with each other, we perform 6D quantum calculation involving all those DOFs. On the contrary, if we assume that the movement of the molecule (x, y, z, and Z) on the plane of the surface is only weakly affected by the COM molecular DOFs (X and Y), such two sets of molecular DOFs ($\{x, y, z, Z\}$ and $\{X, Y\}$) may be termed as 4D⊗2D system (see Figure 2) for mean-field calculation.

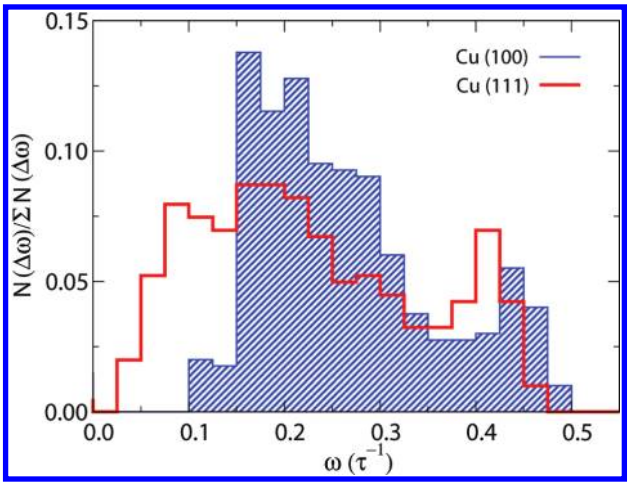

Figure 3. Phonon distribution, $g(\omega) = N(\Delta\omega)/\Sigma N(\Delta\omega)$ for a finite crystal of Cu(100) and Cu(111) as a function of $\omega(\tau^{-1})$ where $\tau = 10^{-14}$ s. The sum runs over all phonon frequencies.

IIIB. PHONON DISTRIBUTION AT A GIVEN SURFACE TEMPERATURE AND THE EFFECTIVE HAMILTONIAN FOR THE MOLECULE−SURFACE SCATTERING

The effective potential, which appears into the above molecular Hamiltonian (eq 2), is derived by taking into account the average over the molecule−surface interaction potential with all possible configurations arising due to the initial state distribution of the phonon modes (see the summation over the initial states, n_k^0 s, in Φ_0^p and thereby, in eq A1) by including either the BP or BEP factor (see Appendix A).

We construct the Hamiltonian (H_0) for the solid atoms by including zeroth- and second-order terms with respect to the displacement from their equilibrium position (i.e., first-order terms are zeros) as

$$H_0 = V_0 + \sum_{k=1}^{3N-6} H_k^0 \qquad (4)$$

where V_0 is the zero point energy and $H_k^0 = {}^1/_2(\dot{Q}_k^2 + \omega_k^2 Q_k^2)$. The $(3N - 6)$ number of nonzero frequencies (ω_k's) are obtained by diagonalizing the force constant (Hessian) matrix of the solid. *The calculated phonon spectrum for Cu(100)/Cu(111) system are presented in* Figure 3.

Because we are interested in exploring the effect of phonon modes on the dissociative chemisorption and scattering processes, it is necessary to evaluate the first and second derivative of the interaction potential to include the phonon forcing and to introduce the self-consistent treatment of the coupling due to the phonon excitation processes to the motion of the molecule. The phonon quantum transitions arise due to the anharmonic terms of the interaction potential (V_I) between gas molecule and surface atoms, where such potential on expansion in terms of phonon coordinates (Q_k's) is given by

$$V_I = V_I^{(0)} + \sum_k V_k^{(1)} Q_k + \frac{1}{2}\sum_{kl} V_{kl}^{(2)} Q_k Q_l + \ldots \qquad (5)$$

where $V_I^{(0)}$ is the interaction potential with the lattice atoms at the equilibrium geometry. The first derivative ($V_k^{(1)}$) and second

derivative ($V_{kl}^{(2)}$) in eq 5 are the cause for phonon excitation due to diatom−surface collision. The normal modes (Q_k) are expressed in terms of boson creation ($b_k^\dagger$)/annihilation (b_k) operators such as $Q_k = A_k(b_k^\dagger + b_k)$ and $A_k = (\hbar/2\omega_k)^{1/2}$. The solution of the TDSE due to the interaction potential up to first-order terms in eq 5 is[54]

$$U_I(t,t_0) = \exp[i(\beta_k(t,t_0) + \alpha_k^+(t,t_0)b_k^\dagger + \alpha_k^-(t,t_0)b_k)] \quad (6)$$

where

$$\alpha_k^\pm(t,t_0) = -\frac{A_k}{\hbar}\int_{t_0}^{t} dt'\, V_k^{(1)}(t') \exp(\pm i\omega_k t') \quad (7a)$$

and

$$\beta_k(t,t_0) = \frac{A_k{}^2}{\hbar^2}\int_{t_0}^{t} dt'\, V_k^{(1)}(t')\int_{t_0}^{t'} dt''\, V_k^{(1)}(t'') \sin[\omega_k(t'-t'')] \quad (7b)$$

The effective potential that governs the motion of the incoming molecule (H_2/D_2) appears as

$$V_{eff} = \langle\Phi|V_I|\Phi\rangle = \langle\Phi_0|U^\dagger V_I U|\Phi_0\rangle \quad (8)$$

and its explicit form is obtained by incorporating the initial state $|\Phi_0\rangle = \Pi_k|n_k^0\rangle$ of the phonons and the time evolution operator, $U = \exp(-i\int dt\, H_0/\hbar)U_I$, as follows:

$$\begin{aligned} V_{eff} &= V_I^{(0)} + \sum_k \omega_k{}^{-1}\varepsilon_k(t) \\ \varepsilon_k(t) &= V_k^{(1)}(t)\int_{t_0}^{t} dt'\, V_k^{(1)}(t') \sin[\omega_k(t'-t)] \end{aligned} \quad (9)$$

Furthermore, we assume that the phonons are initially spread according to either Boltzmann or Bose−Einstein distribution characterized by the surface temperature (T_s) and, thereby, the initial state ($\{n_0\}$) becomes $\Phi_0^p = \Sigma_{\{n0\}}p_{\{n0\}}|\{n_0\}\rangle$, where $p_{\{n0\}} = \Pi_{k=1}^{3N-6}p_{nk0}$. The quantity, p_{nk0}, can be expressed for the BP factor:

$$p_{n_k^0} = z_k^{n_k^0}(1-z_k) \quad (10)$$

or the BEP factor:

$$\begin{aligned} p_{n_k^0} &\propto \frac{1}{\exp(n_k^0\hbar\omega_k\beta) - 1} \\ &= z_k^{n_k^0}(1 - z_k^{n_k^0})^{-1} \\ &= z_k^{n_k^0} + z_k^{2n_k^0} + z_k^{3n_k^0} + z_k^{4n_k^0} + \ldots \end{aligned} \quad (11)$$

where the Boltzmann constant, k_B, appears in the partition function, $z_k = \exp(-\beta\hbar\omega_k)$ with $\beta = 1/k_BT_s$. It is important to note that the so-called low temperature expansion of the BEP factor $[z_k^{n_k^0}(1 - z_k^{n_k^0})^{-1}]$ up to any higher order to achieve the convergence is equally valid both at low ($z_k^{n_k^0} \ll 1$) and at high ($z_k^{n_k^0} < 1$) temperature limits, but the high temperature expansion of the BEP factor $[1/(\exp(n_k^0\hbar\omega_k/k_BT_s) - 1)]$ is valid subject to the numerical magnitude ($n_k^0\hbar\omega_k/k_BT_s \ll 1$) of the argument of the exponential. The convergence of the low temperature expansion of the BEP factor at the high temperature limit could be very slow, but the same is guaranteed by its form with a sufficient number of terms. On the contrary, the high temperature limit is relative with respect to the parameters in the argument $[n_k^0\hbar\omega_k/k_BT_s]$, namely, the initial state quantum number (n_k^0), the frequency of the phonon mode (ω_k), and the surface temperature (T_s). Even for a particular frequency, the high temperature limit changes with the initial quantum number or for a given quantum number, the same limit becomes different with the frequency of the phonon modes. Therefore, it is possible to use the low temperature expansion form of the BEP factor in a robust manner at both low and high temperature limits.

When we incorporate eqs 6, 7, and 10 or 11 in eq 8, we obtain the final expression of the effective potential:[47,48]

$$\begin{aligned} V_{eff} &= \langle\Phi^p|V_I|\Phi^p\rangle = \langle\Phi_0^p|U^\dagger V_I U|\Phi_0^p\rangle \\ &= V_I^{(0)} + \sum_k \eta_k(t,T_s)V_k^{(1)} \end{aligned} \quad (12)$$

where

$$\begin{aligned} \eta_k(t,T_s) = -\frac{1}{\hbar\omega_k}\int dt'\, \frac{d}{d\rho_k}(\Delta E_k^+(T_s) + \Delta E_k^-(T_s)) \\ \times(I_{sk}(t')\sin(\omega_k t') + I_{ck}(t')\cos(\omega_k t')) \end{aligned} \quad (13)$$

with

$$I_{ck}(t) = \int dt'\, \cos(\omega_k t')V_k^{(1)}(t')$$

$$I_{sk}(t) = \int dt'\, \sin(\omega_k t')V_k^{(1)}(t')$$

IIIC. ENERGY TRANSFER FROM MOLECULE TO SURFACE OR VICE VERSA

Considering the Boltzmann or Bose−Einstein distribution of the initial phonon states at a given surface temperature, T_s, the expressions for energy transfer[50] for creation/annihilation processes, $\Delta E_k^\pm$, and total energy transfer, ΔE_{Ph} ($=\Sigma_k(\Delta E_k^+ + \Delta E_k^-)$), are

$$\begin{aligned} \Delta E_k^\pm &= \pm\frac{4\hbar\omega_k}{\rho_k\sqrt{a_k^{(1)}}}(1-z_k)\exp\left(\frac{1}{2}\beta\hbar\omega_k\right)\left(\beta\hbar\omega_k \mp \sqrt{a_k^{(1)}}\right)^{-2} \\ \Delta E_{Ph} &= \sum_k \hbar\omega_k\rho_k\frac{\sinh(\Delta_k)}{\Delta_k} \end{aligned} \quad (14)$$

where $\Delta_k = {}^1/_2\hbar\omega_k\beta$ and

$$\begin{aligned} \Delta E_k^\pm &= \pm\hbar\omega_k\rho_k^{-1}\sum_{n=1}^{\infty} 4a_k^{(n)^{-1/2}} z_k^{-n/2}\left[n\hbar\omega_k\beta \mp \sqrt{a_k^{(n)}}\right]^{-2} \\ \Delta E_{Ph} &= \sum_k k_B T_s\rho_k\sum_{n=1}^{\infty}\frac{x_k^n}{n} \end{aligned} \quad (15)$$

where $x_k = \exp({}^1/_2\beta\hbar\omega_k)$, respectively.

The quantity $a_k^{(n)} = n^2\beta^2\hbar^2\omega_k{}^2 + 4n\beta\hbar\omega_k\rho_k{}^{-1}$ and the excitation strength is defined as $\rho_k = \alpha_k^+\alpha_k^-$. The above expressions for energy transfer from molecule to surface or vice versa due to the choice of BP or BEP factor for the initial state distribution of the phonon modes are formulated in Appendix A and clearly demonstrate that the surface temperature dependence appears only for the BEP case. Because the expression of energy transfer [eq 15] due to the choice of Bose−Einstein distribution for the initial states of the phonon modes depends directly on the BEP factor [eq 11], the truncation of series [n in eq 15] is based on the numerical magnitude of the term, z_k^n ($=x_k^{-n/2}$). *Such truncation is*

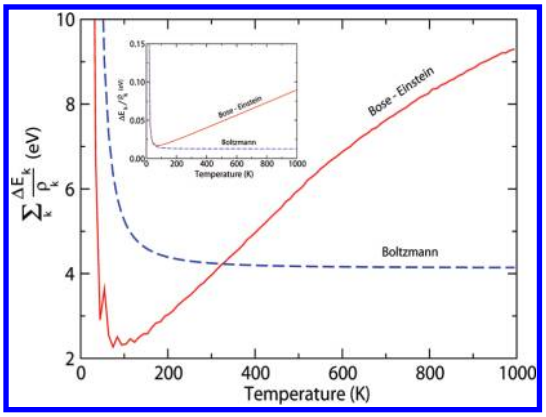

Figure 4. Calculated quantity, $\Sigma_{k=1}^{342}\Delta E_k/\rho_k$ (ω_D = 0.42 τ^{-1}), for all the modes and for a particular mode, $\Delta E_k/\rho_k$, of the Cu(100) crystal (ω_k = 0.18 τ^{-1}, k = 89) using BEP and BP factors are displayed as a function of temperature in the figure and inset, respectively.

nothing but the cutoff due to the Debye frequency at a given temperature. When the surface temperature is low enough, only low frequency phonon modes contribute to the energy transfer, because the series in eq 15 converges very fast only with few terms, i.e., for higher frequency modes, all terms of the series are virtually zeros even at low temperature. In other words, as the temperature of the surface increases, more and more higher frequency modes (up to the Debye frequency) contribute to the phonon energy transfer and to the effective potential.

The energy transfer, ΔE_k, for the kth mode depends both on the initial state distribution through either the BP or BEP factor and on initial KE of the incoming molecule through excitation-strength term, ρ_k, whereas the quantity, $\Delta E_k/\rho_k$, defines a function arising only due to the initial state distribution. When the initial KE of the incoming molecule is very small, the term ρ_k modifies the total energy transfer profile to a negligibly small quantity and the reflection of the initial choice of distribution function has no scope to appear in the sticking and transition probability with the change of surface temperature. In Figure 4, *the functional form of* $\Sigma_k(\Delta E_k)/(\rho_k)$ *due to the phonon modes of Cu(100) surface obtained by BP factor [eq 14] appears to be temperature-independent but the corresponding function obtained by BEP factor [eq 15] increases with the change of surface temperature*. The energy transfer due to any individual mode for both cases (Boltzmann/Bose−Einstein) demonstrates the feature similar to that shown in the inset of Figure 4.

Though we can calculate the total energy of the system by employing eq 2, it is difficult to find the energy of a subsystem (molecule or surface) and, thereby, eq 15 is formulated within harmonic approximation to calculate the energy transfer from molecule to the surface or vice versa. On the contrary, when the molecule is at the asymptote ($Z_0 = \infty$) just before initialization and after completion of the propagation at t = 0 and ∞, respectively, the Hamiltonian (eq 2) practically represents the molecular DOFs only and thus, the difference of the incoming and outgoing molecular energy (eq 16) will represent the "exact" loss or gain of energy by the molecule to or from the solid surface:

$$\Delta E = \left(\frac{\hbar^2 {k_{out}}^2}{2M} + E_{v'j'm_{j'}}\right) - \left(\frac{\hbar^2 {k_{in}}^2}{2M} + E_{vjm_j}\right) \qquad (16)$$

which, in fact, automatically includes the contribution of linear interaction terms responsible for energy transfer from molecule to the surface or vice versa. Calculated energy transfer by eq 16 is expected to be higher or lower in magnitude compared to eq 15.

IVA. TDDVR METHODOLOGY ON MOLECULE−SURFACE SCATTERING

The TDDVR method is a well established[55−66] molecular dynamical simulation approach, which can perform quantum dynamics on systems with many DOFs. At present, we employ TDDVR methodology to investigate the dynamical phenomena originating due to molecule−surface interaction. Though the detailed formulations of the different versions of TDDVR approach are presented successively elsewhere,[55−66] we briefly demonstrate the relevant equations of the latest one to bring the completeness of this article for current perspective in the simplest but completely generalized way. The prime technical point of TDDVR dynamics is the movement of basis functions by using "classical" equations of motion, where the width parameter of the primitive basis set is assumed as time-independent. The adiabatic representation of TDSE for the diatom−surface interaction Hamiltonian [see eq 2] on a single BO surface is

$$i\hbar\frac{\partial}{\partial t}\Psi(\{X_k\},t) = \hat{\mathbf{H}}(\{X_k\},t,T_s)\,\Psi(\{X_k\},t) \qquad (17)$$

where

$$\int \Psi^{\dagger}(\{X_k\},t)\,\Psi(\{X_k\},t)\prod_{k=1}^{p} dX_k = 1 \qquad (18)$$

at any time t and $\{X_k\} \equiv x, y, z, X, Y, Z$. The wave function $[\Psi(\{X_k\}, t)]$ for many DOFs (p) is expanded in terms of products of TDDVR basis functions $[\{\psi_{i_k}(X_k,t)\}]$ for the various kth modes,

$$\Psi(\{X_k\},t) = \sum_{i_1 i_2 \ldots i_p} c_{i_1 i_2 \ldots i_p}(t)\prod_{k=1}^{p}\psi_{i_k}(X_k,t) \qquad (19)$$

and the i_kth basis for the kth mode is again expressed with DVR basis multiplied by plane wave to represent the coordinate, X_k, as a function of time, t,

$$\begin{aligned}\psi_{i_k}(X_k,t) &= \phi(X_k,t)\sum_{n=0}^{N_k}\xi_n^*(x_{i_k})\,\xi_n(x_k)\\ &= \sum_{n=0}^{N_k}\xi_n^*(x_{i_k})\,\Phi_n(X_k,t)\\ \phi(X_k,t) &= \pi^{1/4}\exp\left(\frac{i}{\hbar}\{P_{X_k^c}(t)[X_k - X_k^c(t)]\}\right)\end{aligned} \qquad (20)$$

where harmonic oscillator eigenfunctions are the primitive basis to construct DVR functions,

$$\xi_n(x_k) = \left(\frac{2\,\mathrm{Im}\,A_k}{\pi\hbar}\right)^{1/4}\frac{1}{\sqrt{n!2^n\sqrt{\pi}}}\exp\left(-\frac{{x_k}^2}{2}\right)H_n(x_k) \qquad (21a)$$

$$x_k = \sqrt{\frac{2\,\mathrm{Im}\,A_k}{\hbar}}\,(X_k - X_k^c(t)) \qquad (21b)$$

$$x_{i_k} = \sqrt{\frac{2\,\mathrm{Im}\,A_k}{\hbar}}\,(X_{i_k}(t) - X_k^c(t)) \qquad (21c)$$

A TDDVR grid point, X_{i_k}, is determined by eq 21c using the root, x_{i_k}, of the $(N_k + 1)$th Hermite polynomial, $H_{N_k+1}(x_k)$. Because the roots (x_{i_k}'s) of the polynomial are fixed values, the positions of the TDDVR grid points (X_{i_k}'s) will change as a function of time due to the time-dependent variables, $X_k^c(t)$,

$$X_{i_k}(t) = X_k^c(t) + \sqrt{\frac{\hbar}{2\ \mathrm{Im}\ A_k}}\, x_{i_k} \tag{22}$$

The Gauss−Hermite basis, $\Phi_n(X_k,t)$, for the kth mode as introduced in eq 20 have the following important properties: (a) They form an orthonormal basis,

$$\int \mathrm{d}X_k\ \Phi_m^*(X_k,t)\ \Phi_n(X_k,t) = \delta_{mn}^k \tag{23}$$

(b) The ground state of the GH basis is a Gaussian wave packet (GWP).

The TDDVR basis functions, ψ_{i_k}'s, as defined in eq 19 for the kth mode constitute an unnormalized orthogonal set,

$$\int \mathrm{d}X_k\ \psi_{i_k}^*(X_k,t)\ \psi_{i'_k}(X_k,t) = \delta_{i_k i'_k} A_{i_k i'_k} \tag{24}$$

where A_k is the normalization factor.

When the molecule−surface interaction Hamiltonian (see eq 2) and the TDDVR representation of wave function (eqs 19−21c) are substituted into the TDSE (eq 17), the classical path picture appears naturally along with the quantum equation of motion. The compact form of TDDVR matrix equation for quantum motion can be derived by employing time-dependent variational principle[67] as given below:

$$\mathrm{i}\hbar\mathbf{A}\dot{C} = \mathbf{H}^{\mathrm{t}}\mathbf{C} \tag{25}$$

and the matrix equation under a similarity transformation takes the following convenient form

$$\mathrm{i}\hbar\dot{\mathbf{D}}(\mathbf{t}) = \mathbf{A}^{-1/2}\mathbf{H}^{\mathrm{t}}\mathbf{A}^{-1/2}\mathbf{D} \tag{26}$$

where $\mathbf{D} = \mathbf{A}^{1/2}\mathbf{C}$. The explicit expression of the differential equation for an amplitude, $d_{i_1 i_2 \ldots i_p}$, is

$$\begin{aligned}\mathrm{i}\hbar\dot{d}_{i_1 i_2 \ldots i_p} &= \frac{1}{2}\left\{\sum_k \dot{P}_{X_k^c}\sqrt{\frac{\hbar}{\mathrm{Im}\ A_k}}\,\bar{G}_{i_k i_k}\right\} d_{i_1 i_2 \ldots i_p} \\ &+ \left\{\sum_k \frac{m_k(\dot{X}_k^c)^2}{2}\right\} d_{i_1 i_2 \ldots i_p} - \sum_k \left\{\frac{\hbar\ \mathrm{Im}\ A_k}{2\mu}\sum_{i'_1 i'_2 \ldots i'_p}\{\bar{F}_{i_k i'_k}\} d_{i'_1 i'_2 \ldots i'_p}\prod_{k'\neq k}^{p}\delta_{i_{k'} i'_{k'}}\right\} \\ &+ V_0(\{X_{i_k}\}) d_{i_1 i_2 \ldots i_p} + V_{\mathrm{eff}}(\{X_{i_k}\},t,T_s) d_{i_1 i_2 \ldots i_p}\end{aligned} \tag{27}$$

The explicit expression of the component matrices ($\mathbf{D}$, $\mathbf{A}$, $\mathbf{G}$, and $\mathbf{F}$) of TDDVR equation of motion are presented in Appendix B. The contribution of different modes on a time-dependent amplitude ($\dot{d}_{i_1 i_2 \ldots i_p}$) can be evaluated independently, i.e., $\mathbf{F}_k$ matrix couple grid points or basis functions of the kth mode only. This feature allows *parallelization of the algorithm*,[63] reduces computational cost *remarkably*,[63−66] and paves the possibility to pursue relatively large dimensional calculations. On the other hand, the classical path equations for the k th mode, those appear along with the quantum equation of motion, can be written as

$$\dot{X}_k^c(t) = \frac{P_{X_k^c}(t)}{m_k} \tag{28}$$

$$\dot{P}_{X_k^c}(t) = -\left.\frac{\mathrm{d}V(\{X_k\})}{\mathrm{d}X_k}\right|_{X_k(t)=X_k^c(t)} + X_k^F(t) \tag{29}$$

where m_k is either the reduced (μ) or the total (M) mass of the diatom and $X_k^F(t)$ is the quantum force. A rigorous expression of $X_k^F(t)$ is derived by using Dirac−Frenkel variational principle,[67] i.e., by minimizing the following integral with respect to $P_{X_k^c}$,

$$\begin{aligned}I = \int &\left(-\mathrm{i}\hbar\frac{\partial\Psi^*(\{X_k\},t)}{\partial t} - H(\{P_{X_k}\},\{X_k\})\Psi^*(\{X_k\},t)\right) \\ &\times\left(\mathrm{i}\hbar\frac{\partial\Psi(\{X_k\},t)}{\partial t} - H(\{P_{X_k}\},\{X_k\})\Psi(\{X_k\},t)\right)\prod_{k=1}^{p}\mathrm{d}X_k\end{aligned}$$

The explicit expression of $X_k^F(t)$ thus obtained is

$$\begin{aligned}X_k^F(t) = &\sum_{i_1 i_2 \ldots i_k i'_k \ldots i_p} c^*_{i_1 i_2 \ldots i_k \ldots i_p}(t)\, c_{i_1 i_2 \ldots i'_k \ldots i_p}(t) \\ &\times\left\{\frac{2(\mathrm{Im}\ A_k)^2}{\mu}\left[S^{(2)}_{i_k i'_k}\frac{S^{(1)*}_{i_k i_k}}{A_{i_k i_k}} - S^{(3)}_{i_k i'_k}\right]\right. \\ &\left. - \frac{\hbar\ \mathrm{Im}\ A_k}{\mu}\left[R_{i_k i'_k}\frac{S^{(1)*}_{i_k i_k}}{A_{i_k i_k}} - T^*_{i_k i'_k}\right]\right\} \\ &\Big/\left[\sum_{i_1 i_2 \ldots i_k \ldots i_p} c^*_{i_1 i_2 \ldots i_k \ldots i_p}(t) c_{i_1 i_2 \ldots i_k \ldots i_p}(t)\frac{S^{(1)*}_{i_k i_k} S^{(1)}_{i_k i_k}}{A_{i_k i_k}}\right. \\ &\left. - \sum_{i_1 i_2 \ldots i_k i'_k \ldots i_p} c^*_{i_1 i_2 \ldots i_k \ldots i_p}(t) c_{i_1 i_2 \ldots i'_k \ldots i_p}(t) S^{*(2)}_{i_k i'_k}\right]\end{aligned} \tag{30}$$

where the matrices, R, $S^{(n)}$, and T are time-independent [see Appendix B] and need to be calculated once for all the time. It is important to note that the time-dependence of X_k^F arises from the time-dependent coefficients $\{c_{i_1 i_2 \ldots i_k \ldots i_p}(t)\}$ only.

IVB. INITIALIZATION, PROPAGATION, AND PROJECTION

Because we perform 6D quantum calculations on an effective Hamiltonian (see eq 2) that defines molecule−surface interaction including the effect of phonon modes, the initial wave function could be represented as

$$\begin{aligned}&\Psi(x,y,z,X,Y,Z,t_0) \\ &= \frac{1}{r} g_v(r)\ Y_{jm_j}(\theta,\phi)\ \Phi_{\mathrm{GWP}}(X,t_0)\ \Phi_{\mathrm{GWP}}(Y,t_0)\ \Phi_{\mathrm{GWP}}(Z,t_0)\end{aligned} \tag{31}$$

where r is the bond distance, the polar angles θ and ϕ specify the orientation of the diatomic molecule, $g_v(r)$ is the Morse eigenfunction, and Y_{jm_j} is a spherical harmonics. The Cartesian coordinates (x, y, and z) are related with polar ones (r, θ, and ϕ) through standard transformation. The GWP ($\Phi_{\mathrm{GWP}}(Z,t_0)$) for the Z coordinate represents the translational wave function for the COM of the incoming diatom with a initial momentum,

dx.doi.org/10.1021/jp201524x |J. Phys. Chem. A 2011, 115, 5256–5273

p_0 (=$\hbar k_0$), where the corresponding wavevector (k_0) appears in its plane wave component as given below:

$$\Phi_{GWP}(Z,t_0) = \left[2\pi{\Delta_Z}^2\left(1+\frac{\hbar^2{t_{foc}}^2}{4M^2{\Delta_Z}^4}\right)\right]^{-1/4}\exp\left(-\frac{(Z-Z_{foc}-\hbar k_0 t_{foc}/M)^2}{4{\Delta_Z}^2-2i\hbar t_{foc}/M}-ik_0Z\right) \quad (32)$$

The wavepacket is initially centered around Z_0, where t_{foc} is the time at which the GWP is focused around Z_{foc} with a width Δ_Z (=$^1/_2(\hbar/\mathrm{Im}\ A_Z)^{1/2}$). On the contrary, as the initial wave function should be spread uniformly over the $X-Y$ plane, we introduce $\Phi_{GWP}(X,t_0)$ and $\Phi_{GWP}(Y,t_0)$ for the X and Y coordinates without any specific momentum component unlike the second term in the exponent of eq 32 for the $\Phi_{GWP}(Z,t_0)$. In other words, because a GWP can be expressed as the sum of infinite number of plane waves with all possible momentum components, the $\Phi_{GWP}(X,t_0)$ and $\Phi_{GWP}(Y,t_0)$ will present the space (X, Y) uniformly.

The initial wave function [eq 31] can be expressed in terms of TDDVR basis functions as given below:

$$\begin{aligned}\Psi(x,y,z,X,Y,Z,t_0) &= \sum_{IJKLMN} C_{IJKLMN}(t_0)\,\psi_I(x)\,\psi_J(y)\,\psi_K(z)\,\psi_L(X)\,\psi_M(Y)\,\psi_N(Z)\\ &= \frac{1}{r}g_v(r)\,Y_{jm_j}(\theta,\phi)\,\Phi_{GWP}(X,t_0)\,\Phi_{GWP}(Y,t_0)\,\Phi_{GWP}(Z,t_0)\end{aligned} \quad (33)$$

If we define the amplitude of the wave function only at the TDDVR grid points, the function takes the following form due to orthogonality relationship of the basis functions (see eq 24) known at the grid points:

$$\begin{aligned}\Psi(x_I,y_J,z_K,X_L,Y_M,Z_N,t_0) &= \frac{C_{IJKLMN}(t_0)}{\mathrm{Im}\ A}A^x_{II}A^y_{JJ}A^z_{KK}A^X_{LL}A^Y_{MM}A^Z_{NN}\\ &= \frac{g_v(r_{IJK})}{r_{IJK}}Y_{jm_j}(\theta_{IJK},\phi_{IJK})\,\Phi_{GWP}(X_L,t_0)\,\Phi_{GWP}(Y_M,t_0)\,\Phi_{GWP}(Z_N,t_0)\end{aligned} \quad (34)$$

which in turn gives the following expression for the initial amplitude of the wave function:

$$d_{IJKLMN}(t_0) = \mathrm{Im}\ A\frac{\frac{1}{r_{IJK}}g_v(r_{IJK})\,Y_{jm_j}(\theta_{IJK},\phi_{IJK})}{\sqrt{A^x_{II}A^y_{JJ}A^z_{KK}A^X_{LL}A^Y_{MM}A^Z_{NN}}}\Phi_{GWP}(X_L,t_0)\,\Phi_{GWP}(Y_M,t_0)\,\Phi_{GWP}(Z_N,t_0)$$

where $\mathrm{Im}\ A = (\hbar/2)^{3/2}(\mathrm{Im}\ A_x\,\mathrm{Im}\ A_y\,\mathrm{Im}\ A_z\,\mathrm{Im}\ A_X\,\mathrm{Im}\ A_Y\,\mathrm{Im}\ A_Z)^{-1/4}$.

If we are interested in the dissociative chemisorption probability, one can simply sum over the amplitudes defined on the grid points with bond distance r larger than a critical value r^*, i.e.,

$$P_{diss} = \sum_{p=1}^{N_d}|d_p|^2 h(r_p - r^*) \quad (35)$$

where $h(x)$ is a Heaviside function becomes unity for positive and zero for negative arguments. The value of r_p is obtained as

$$r_p = \sqrt{{x_I}^2+{y_J}^2+{z_K}^2} \quad (36)$$

where I, J, and K run over the grid points in the three Cartesian coordinates. The critical distance is the smallest separation between two holes at which the hydrogen atoms can be chemisorbed on the surface. The sticking probability[32,33] includes the physisorption and chemisorption processes, i.e., $P_{stick} = P_{diss} + P_{ads}$, where P_{ads} contains processes by which the molecule as such is adsorbed with bond distances less than r^* and Z^*, i.e.

$$P_{ads} = \sum_{p=1}^{N_d}|d_p|^2 h(r_p - r^*)\,h(Z^* - Z_p) \quad (37)$$

When the scattered wave function is far away from the interaction region, the energy resolved elastic/inelastic state to state transition probabilities can be calculated as the ratio of the outgoing ($C^+_{k_{out},v'j'm_{j'}}$) and the incoming ($C^-_{k_{in},vjm_j}$) fluxes:

$$P^{v'j'm_{j'}}_{vjm_j}(E) = \frac{\frac{k_{out}}{M}\left|C^+_{k_{out},v'j'm_{j'}}\right|^2}{\frac{k_{in}}{M}\left|C^-_{k_{in},vjm_j}\right|^2} \quad (38)$$

where

$$C^+_{k_{out},v'j'm_{j'}} = \frac{1}{(2\pi)^{3/2}}\mathrm{Im}\ A\sum_{IJKLMN}\left(\frac{d_{IJKLMN}}{\sqrt{A^x_{II}A^y_{JJ}A^z_{KK}A^X_{LL}A^Y_{MM}A^Z_{NN}}}\right)\times\frac{1}{r_{IJK}}g^*_{v'}(r_{IJK})\,Y^*_{j'm_{j'}}(\theta_{IJK},\phi_{IJK})\exp(-ik_{out}Z_N)\exp\left\{\frac{i}{\hbar}[P_{Z_c}(Z_N-Z_c)]\right\} \quad (39a)$$

$$C^-_{k_{in},vjm_j} = \left(\frac{2}{\pi}\right)^{1/4}\left(\frac{1}{2\pi}\right)\mathrm{Im}\ A\sqrt{\Delta_Z}\exp[i(k_{in}-k_0)Z_c - {\Delta_Z}^2(k_{in}-k_0)^2]\times\frac{\frac{1}{r_{IJK}}g_v(r_{IJK})\,Y_{jm_j}(\theta_{IJK},\phi_{IJK})}{\sqrt{A^x_{II}A^y_{JJ}A^z_{KK}A^X_{LL}A^Y_{MM}}}\Phi_{GWP}(X,t_0)\,\Phi_{GWP}(Y,t_0) \quad (39b)$$

The energy resolved state to state transition probabilities obey the following detailed energy balance equation:

$$\frac{\hbar^2{k_{in}}^2}{2M}+E_{vjm_j} = \frac{\hbar^2{k_{out}}^2}{2M}+E_{v'j'm_{j'}} \quad (40)$$

where k_{in} and k_{out} indicate the incoming and outgoing wave vectors, respectively. The sticking probability ($P_{stick}(E)$) can also be defined as

$$P_{stick}(E) = 1 - \sum_{v'j'm_{j'}}P^{v'j'm_{j'}}_{vjm_j}(E) \quad (41)$$

The asymptotic wave function of a particular trajectory is analyzed by using eqs 38 and 41 to obtain $P^{v'j'm_{j'}}_{vjmj}(E)$ and $P_{stick}(E)$.

IVC. NUMERICAL DETAILS

We set up the equations of motion [eqs 27−29] by involving the following number of TDDVR basis functions, N_x = 28, N_y = 28, N_z = 28, N_X = 10, N_Y = 10, and N_Z = 24 for the molecular coordinates x, y, z, X, Y, and Z, respectively, and solve those coupled differential equations by Lanczos time propagation technique.[68] Such a huge number of basis function ($\sim 5\times 10^7$) is the minimum requirement to achieve converged reaction as well as transition probability. Figure 5a represents the convergence of the calculated average distance ($\langle Z(t)\rangle$) from the COM position of the diatom to the

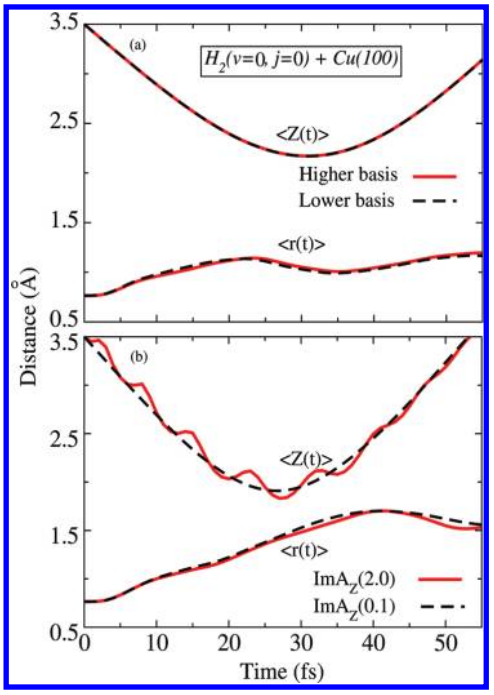

Figure 5. Average distance ($\langle Z(t)\rangle$) from the COM position of the $H_2(v=0,j=0)$ to the top layer of the Cu(100) surface and bond length ($\langle r(t)\rangle$) of the diatom as function of time (a) for collisional energy 0.40 eV with higher (solid line) and lower (dashed line) numbers of basis functions and (b) for collisional energy 0.70 eV with Im A_Z values 2.0 amu τ^{-1} (solid line) and 0.1 amu τ^{-1} (dashed line) including higher number of basis function only.

top layer of the Cu surface and bond length ($\langle r(t)\rangle$) of H_2 as function of time for collisional energy 0.40 eV with higher ($N_x = 28$, $N_y = 28$, $N_z = 28$, $N_X = 10$, $N_Y = 10$, and $N_Z = 24$) and lower ($N_x = 22$, $N_y = 22$, $N_z = 22$, $N_X = 8$, $N_Y = 8$, and $N_Z = 20$) number of basis functions. Though the calculated results could appear sensitive with the numerical magnitude of the imaginary part of the width parameter, particularly, for lower number of basis functions on the incoming molecular coordinate Z (Im A_Z), such sensitivity goes away with a higher number of basis function. As, for example, when we have carried out the dynamics with two widely different numerical magnitudes of the width parameters, namely, Im A_Z = 0.1 and 2.0 amu τ^{-1} ($1\tau = 10^{-14}$ s) but with a higher number of TDDVR basis function to explore the stability of convergence, it achieves the same level of accuracy as shown in the Figure 5b. In one case (Im $A_Z = 0.1$ amu τ^{-1}), the energy spread for the incoming GWP on the Z coordinate covers a large range and in the other case (Im $A_Z = 2.0$ amu τ^{-1}), it is narrow around the collisional energy. It is important to mention that we have calculated the sticking probabilities by using eq 41 and cross-verified the same quantity with the sum of calculated dissociation (P_{diss} [eq 35]) and adsorption (P_{ads} [eq 37]) probabilities, where r^* and Z^* are approximately taken as 2.0 and 1.5 Å, respectively.

Finally, we mention that all the calculations are performed on a *Supermicro SuperServer 8025C-3RB* cluster, where our parallelized equation of motion [eq 27] takes six (6) CPUs at a time for carrying out the quantum-classical dynamics.

V. RESULTS AND DISCUSSION

We carry out quantum dynamics on an effective Hamiltonian (6D) formulated by using BEP factor for initial state distribution

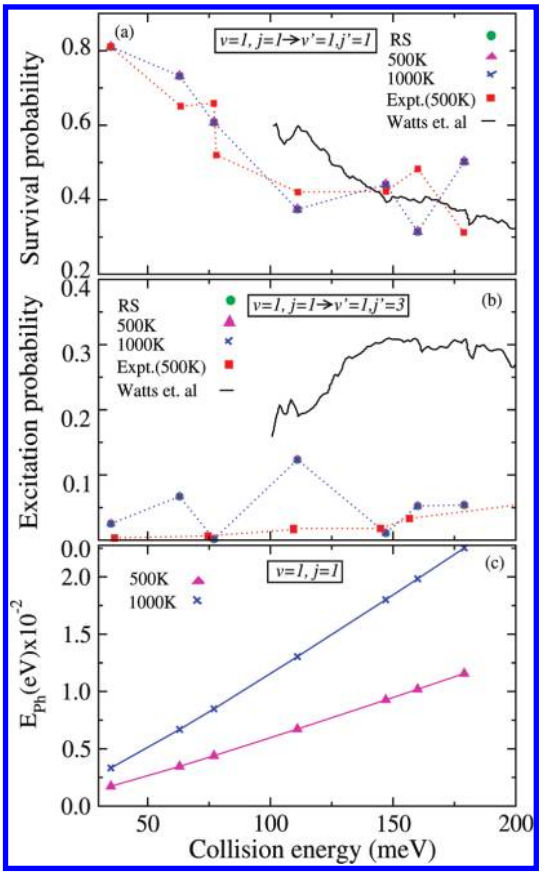

Figure 6. Calculated (a) survival probability ($v = 1, j = 1 \rightarrow v' = 1, j' = 1$) and (b) excitation probability ($v = 1, j = 1 \rightarrow v' = 1, j' = 3$) of H_2 colliding with the Cu(100) surface as a function of collision energy. The experimental and previous theoretical results are adopted from refs 4 and 39, respectively. The energy transfer (ΔE_{Ph}) within harmonic approximation at asymptotic time as functions of collision energy is depicted in panel (c). The effective Hamiltonian is constructed by employing the BEP factor.

of the phonon modes to incorporate the effect of surface temperature, where the workability of TDDVR methodology[55−66] to solve 6D TDSE has been demonstrated by comparing the calculated reaction and transition probabilities with experimental data and then, the effect of phonon modes on those quantities has been displayed.

$H_2(v=1,j=1)-Cu(100)$: In Figure 6, we present the (6D) TDDVR computed (a) survival ($v' = 1, j' = 1$) and (b) excitation ($v' = 1, j' = 3$) probabilities of the incoming $H_2(v=1,j=1)$ molecule colliding with the Cu(100) surface as function of initial KE either by considering RS or by including the phonon modes at different surface temperatures (T_s = 500 and 1000 K) and compare those quantities (survival/excitation) with the experimentally measured[4] probabilities at T_s = 500 K. In these figures, we also display the theoretically computed (6D) probabilities considering RS[51−53] by Watts et al.[39] to demonstrate the accuracy of EDIM potential[23] fitted with DFT-GGA data[21] as well as the workability of TDDVR methodology. In summary, Figure 6 shows the following (a) The experimental survival probabilities ($v = 1, j = 1 \rightarrow v' = 1, j' = 1$) have reasonably good agreement with our results over the entire collisional energy range as well as with the probabilities obtained by Watts et al.[39] Indeed, Watts et al.[39] calculated those probabilities only at the higher energy regions.

dx.doi.org/10.1021/jp201524x |J. Phys. Chem. A 2011, 115, 5256–5273

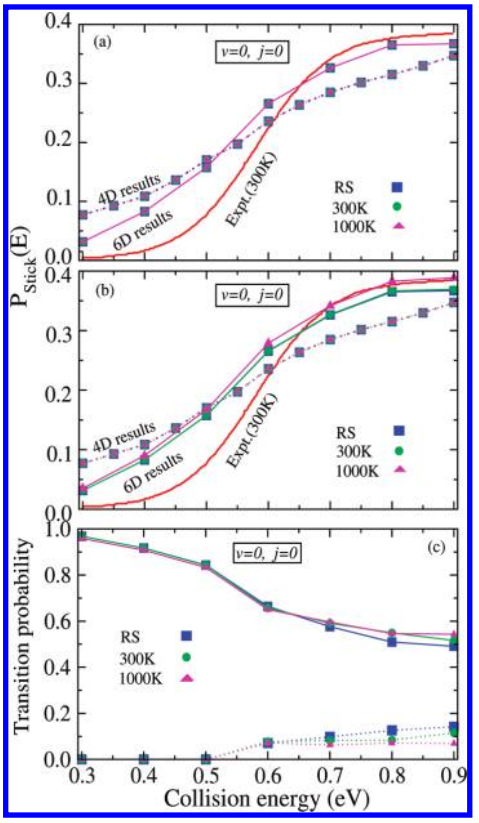

Figure 7. Calculated sticking probability ($P_{stick}(E)$) using 4D⊗2D as well as 6D quantum dynamics considering the (a) BP and (b) BEP factor in the case of the $H_2(v{=}0,j{=}0)-Cu(100)$ system as functions of initial collisional energy, where experimental results are taken from ref 6. The energy resolved state-to-state transition probabilities for vibrationally elastic, $v = 0 \rightarrow v' = 0$ (solid line) and inelastic, $v = 0 \rightarrow v' = 1$ (dashed line) collisions of the same system are presented in panel c.

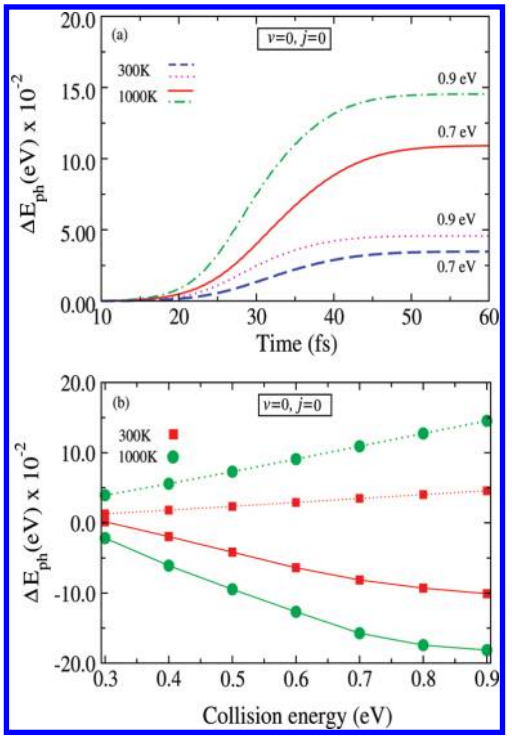

Figure 8. At 300 and 1000 K for $H_2(v{=}0,j{=}0)/Cu(100)$ system, (a) the energy transfer (ΔE_{Ph}) within the harmonic approximation as functions of time with 0.70 and 0.90 eV collision energy and (upper panel of b) the energy transfer (ΔE_{Ph}) at asymptotic time as function of initial kinetic energy (dotted line). The "exact" energy transfer (solid line) calculated by exploiting the detailed balance eq 16 as functions of initial kinetic energy is depicted in the lower part of panel b. The effective Hamiltonian has been formulated by using the BEP factor.

(b) The theoretically calculated excitation ($v = 1, j = 1 \rightarrow v' = 1, j' = 3$) probabilities by employing our methodology and Watts et al.[39] deviate substantially from experimental results, but the computed profile at present appears closer one. It is important to mention that our calculated survival/excitation probabilities are more or less independent with the change of surface temperature and this feature could be explained by monitoring the overall energy transfer (ΔE_{Ph}) from the molecule to the surface at various surface temperatures as function of initial KE [Figure 6c] of the incoming molecule. Because the amount of energy transfer calculated within the harmonic approximation is only ~22 meV even with the highest initial KE (179 meV) of the incoming molecule, it is obvious that both the survival and excitation probabilities remain unchanged with the variation of surface temperature.

$H_2(v{=}0,j{=}0)-Cu(100)$: When we perform the 4D⊗2D and 6D quantum dynamics on an effective potential derived by using BP factor for the initial state distribution of the phonon modes, Figure 7a displays the calculated sticking probabilities for the incoming $H_2(v{=}0,j{=}0)$ molecule on Cu(100) surface as a function of various initial KEs considering the RS as well as the surface with phonon modes at different temperatures (T_s = 300 and 1000 K). The computed sticking probabilities obtained from 6D quantum dynamics show fairly good agreement at higher energies with the fitted reaction probabilities[6] of the experimentally measured data[3] at T_s = 300 K, but 4D⊗2D results do not follow the experimental profile neither at lower nor at higher collisional energy region. Moreover, in both cases, the calculated results fail to show any temperature dependence, as predicted in Figure 4. On the contrary, as we use the BEP factor to construct the effective potential and carry out the dynamics on such effective Hamiltonian, the 6D computed sticking probability [Figure 7b] depicts a noticeable temperature dependence, particularly, at higher energies but the corresponding 4D⊗2D dynamics [Figure 7b] could not bring any signature of similar change with temperature. Therefore, to incorporate the temperature dependence on the sticking probabilities, all the molecular coordinates need to be treated in a fully correlated manner (6D) while performing dynamics on the BEP based effective Hamiltonian. Again, Figure 7c demonstrates the 6D calculated transition probabilities by considering the RS as well as the surface at two temperatures (300 and 1000 K). As the surface temperature increases, these profiles remain the same up to the initial KE 0.6 eV but behave differently from 0.6 to 0.9 eV; namely, the survival and excitation probabilities increase and decrease, respectively. To understand the behavior of reaction and transition probabilities as a function of collisional energies for different surface temperatures, we explore the energy transfer profiles from diatom to the solid or vice versa along with their possible interpretations:

(A) As the diatom approaches the surface from infinity [Z_0 = 3.5 (Å)], there is a threshold time (20 fs) to see the energy transfer calculated within the harmonic approximation [see eq 15] and then, such transfer happens quickly between 25 and 45 fs before it reaches a plateau around 50−60 fs [see Figure 8a]. The same figure demonstrates a sharp increase of energy exchange as the

dx.doi.org/10.1021/jp201524x |J. Phys. Chem. A 2011, 115, 5256–5273

temperature rises for any specific collisional energy and also shows a substantial increase with higher initial kinetic energy for a fixed surface temperature. Moreover, when the molecule is already scattered back to the asymptotic region of Z coordinate at around 60 fs, the upper part of Figure 8b depicts the gain of energy by the surface from the molecule (see eq 15) at two different surface temperatures as functions of initial translational energy.

(B) Because eq 15 for calculating energy transfer from molecule to surface is derived within harmonic approximation, it is expected that such an equation will either decrease or increase the estimate of the actual energy transfer from the molecule to the surface or vice versa (see upper part of Figure 8b). Therefore, we have used an equation [eq 16] that basically provides the detailed balance of energy for incoming and outgoing molecules only, to calculate the "exact" loss of energy from the molecule to the surface. The lower part of Figure 8b shows the profile of energy loss as a function of initial KEs at various surface temperature. This figure also demonstrates a saturation on the profile of energy transfer at higher collisional energy and temperature. The absence of saturation in the upper part of Figure 8b is due to the harmonic approximation involved in the formulation of energy transfer equation [eq 15].

(C) Because the amount of energy transfer is about 0.17 eV (Figure 8) with an initial kinetic energy 0.9 eV, it is sufficient to affect the transition probabilities (Figure 7c) only within the first two vibrational states, namely, $v' = 0$ and 1, at various surface temperatures, where the sticking probability (Figure 7b) as a function of initial KEs shows a noticeable change with temperature for the $H_2(v=0,j=0)-Cu(100)$ system. As a matter of fact, the profile for the loss of energy from the molecule as function of collision energy and its saturation at various surface temperatures may provide an explanation for the contrasting feature of survival and excitation probabilities at lower and higher temperatures.

(D) The advantage of Bose−Einstein based approach over the Boltzmann to capture the effect of surface temperature on the molecular DOFs could be due to the treatment of phonon modes as indistinguishable particles rather than distinguishable ones. As the temperature changes, the average occupation number of the phonons in a quantum state undergoes a change with the BEP based approach rather than the specific occupation number in the case of BP. In other words, while taking the average over the initial states (n_k^{0}'s) arising due to all possible configurations of the phonon modes to calculate the energy transfer to the final states (n_k's), the creation process virtually balances the annihilation one in case of the BP [see Figure 9a], whereas with the BEP factor, creation dominates over the annihilation [see Figure 9b] within the range of initial kinetic energy of the diatom and surface temperature of our investigation.

$D_2(v=0,j=0)-Cu(111)$: When we carry out the 4D⊗2D and 6D quantum dynamics on an effective Hamiltonian constructed by using the BEP factor for the initial state distribution of the phonon modes to explore the collision of $D_2(v=0,j=0)$ on the Cu(111) surface, parts a and b of Figure 10 demonstrate that both 4D⊗2D and 6D quantum dynamics bring noticeable and clear temperature-dependent sticking probabilities, respectively, as a function of initial translational energy of the incoming diatom. Because the amount of energy transfer is about 0.40 eV (Figure 10c) with initial kinetic energy 0.9 eV, the sticking probability (Figure 10a,b) as a function of initial KEs shows a noticeable and substantial change with temperature. The effect of surface temperature on the sticking probability is more prominent in the 6D calculation than 4D⊗2D, indicating the importance of dynamical correlation between the two sets of

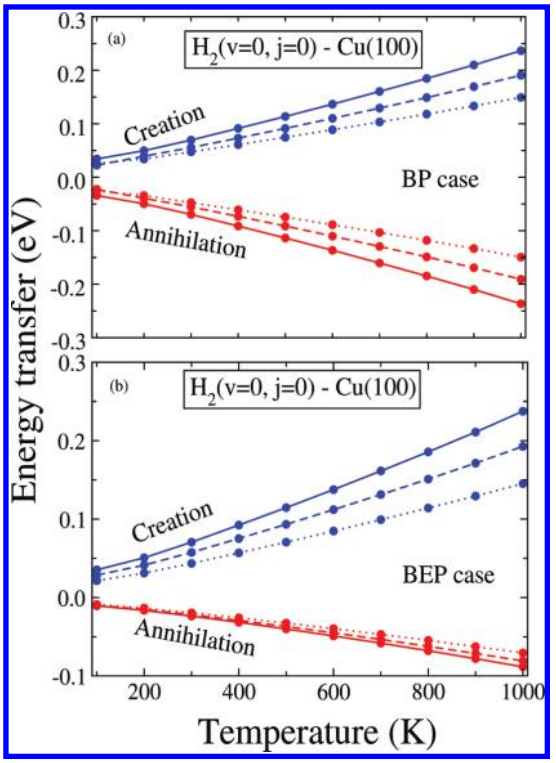

Figure 9. Energy transfer ($\Delta E_{Ph}^{\pm}$) at asymptotic time through creation and annihilation processes for the $H_2(v=0,j=0)/Cu(100)$ system as functions of temperature with 0.50 (dotted line), 0.70 (dashed line), and 0.90 eV (solid line) collision energy considering (a) BP and (b) BEP factor.

molecular coordinates, (x, y, z, Z and X, Y). At this point, we mention that the calculated (6D) sticking probabilities deviate from the experimental results over the entire energy range (see the inset in Figure 10b), probably, due to the lower estimated EDIM fit bth barrier height (see Table 2).

$H_2(v=1,j=0)-Cu(100)$: We again perform 6D quantum dynamics on an effective Hamiltonian derived by invoking the BEP factor for the initial state distribution of the phonon modes and calculate reaction and transition probabilities of the incoming H_2 molecule with initial state $v = 1$ and $j = 0$ colliding with Cu(100) surface as a function of different initial collisional energies considering the RS and the surface including phonon modes at temperatures, 300 and 1000 K. Figure 11a presents the temperature-dependent sticking probabilities along with the fitted profile[6] of the experimentally measured reaction probabilities[3] at 300 K and clearly demonstrates the lower estimation of experimental results by the calculated ones for majority of the collisional energies except at smaller and higher translational energies. Figure 11b depicts the vibrational survival ($v' = 1$) and de-excitation ($v' = 0$) probabilities as a function of initial KEs for the RS and the surface with different temperatures, 300 and 1000 K, where the elastic/inelastic transition probabilities undergo noticeable change from the RS to the surface including phonon modes at different temperatures. Figure 12 shows the rovibrational elastic/inelastic transition probabilities as a function of initial KEs and displays substantial difference from the RS to the surface with various temperatures. In Figures 11b and 12, vibrational and rovibrational transition probabilities calculated at 300 and 1000 K surface temperatures are more or less the same with RS results up to the initial translational energy, 0.4 eV and then, become huge different from each other between 0.4 and 0.65 eV; i.e., the survival and

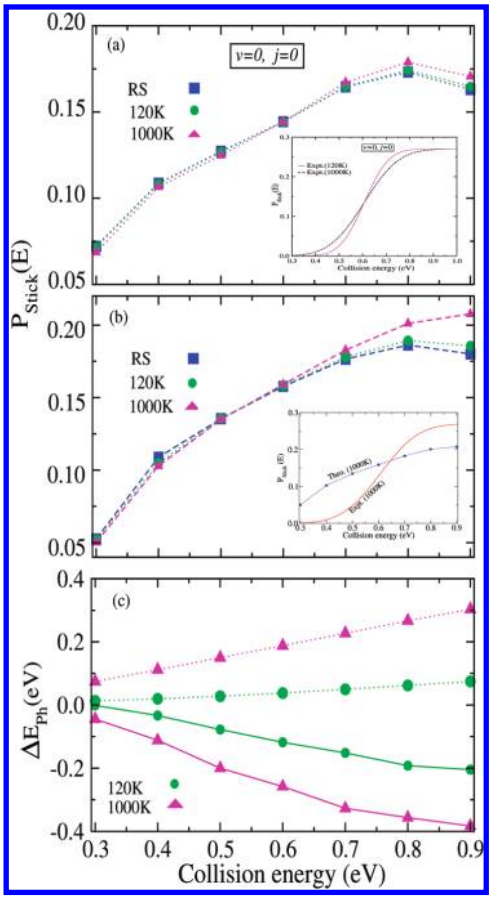

Figure 10. Calculated sticking probabilities ($P_{stick}(E)$) of $D_2(v=0,j=0)$ on the Cu(111) surface using (a) 4D⊗2D and (b) 6D dynamics displayed as functions of initial collisional energy. Experimental results (unnormalized) are presented in the inset. Those experimental data are extracted by employing the fitting equation 7a and normalized data in Figure 3 of ref 8. The upper and lower parts of panel c depict the energy transfer (ΔE_{Ph}) at asymptotic time within the harmonic approximation (dotted line) and the "exact" energy transfer (solid line) calculated by exploiting the detailed balance eq 16, respectively, as functions of initial kinetic energy. The effective Hamiltonian has been derived by employing BEP factor at 120 and 1000 K.

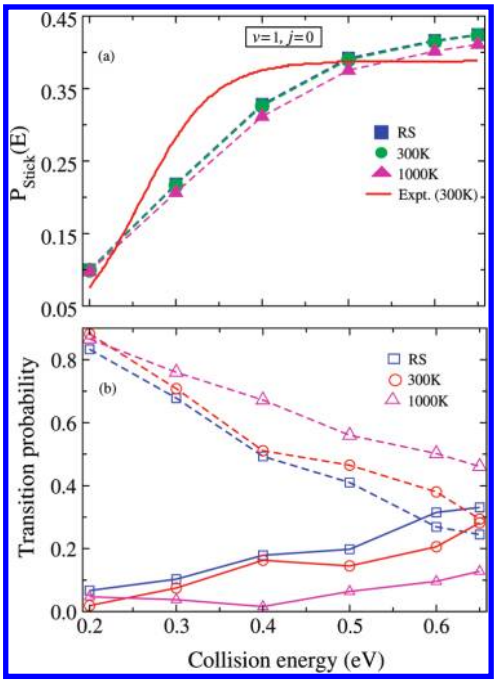

Figure 11. (a) Calculated sticking probability ($P_{stick}(E)$) for $H_2(v=1, j=0)$ on the Cu(100) surface as a function of initial collisional energy, where experimental results are obtained from ref 6. (b) Energy resolved state-to-state transition probabilities for vibrationally inelastic, $v = 1 \rightarrow v' = 0$ (solid line), and elastic, $v = 1 \rightarrow v' = 1$ (dashed line), collisions of the same system. The effective Hamiltonian has been constructed by employing BEP factor at 300 and 1000 K.

de-excitation probabilities increase and decrease as the temperature of the surface increases. It is quite reasonable to explain the noticeable and substantial temperature dependence of reaction and transition probabilities, respectively, in terms of energy transfer (from the diatom to the solid) calculated either within the harmonic approximation or by using the detailed balance of energy between incoming and outgoing molecule. Figure 13 displays the phonon energy transfer profiles as functions of initial KEs calculated at surface temperatures 300 and 1000 K, where the upper and lower parts of the same figure are calculated by employing eqs 15 and 16, respectively. The overall amount of energy transferred due to the inclusion of phonon modes for specific initial collisional energy and temperature appears sufficient to increase/decrease the transition probabilities as well as to affect the sticking probabilities.

VI. SUMMARY

We have presented the detailed formulation to include the effect of phonon modes on the 6D molecular Hamiltonian [see eq 2] that governs the molecule−surface scattering processes, namely, chemisorption, physisorption, and energy resolved state-to-state elastic/inelastic scattering cross-sections. This derivation has been carried out by considering a mean-field approach [see eq 1], where the dynamics of surface modes is incorporated through a second quantization based technique and the parametric dependence of temperature enters into the effective Hamiltonian either by including the BP or by incorporating the BEP factor for the initial states distribution of the surface modes [see Appendix A]. *Such BEP based formulation is the first attempt to account the effect of phonon modes on the 6D molecule−surface scattering Hamiltonian.* Though we include all the modes representing the metal surface [Cu(100)/Cu(111)] and all possible configurations arising due to the phonon states to explore the temperature dependence on the reaction and inelastic transition probabilities quantitatively, the correlation between the molecule and the phonon modes has been considered only within the mean-field approximation to keep the calculations tractable and to access, at what extent, such approximate approach can take into account the effect of phonon modes on the molecular DOFs.

At this junction, we wish to reiterate that the TDDVR method,[55−66] which has been employed to perform 6D quantum dynamics on molecule−surface scattering processes appears to be a good compromise between accuracy and speed. The computed survival ($v' = 1, j' = 1$) and excitation ($v' = 1, j' = 3$) probabilities for $H_2(v=1,j=1)$−Cu(100) collision on an effective Hamiltonian (constructed with BEP factor) show some agreements and disagreements with the experimental results within the collisional energy range, 35−179 meV, and thereby, demonstrate that the EDIM potential[23] fitted with DFT-GGA data[21]

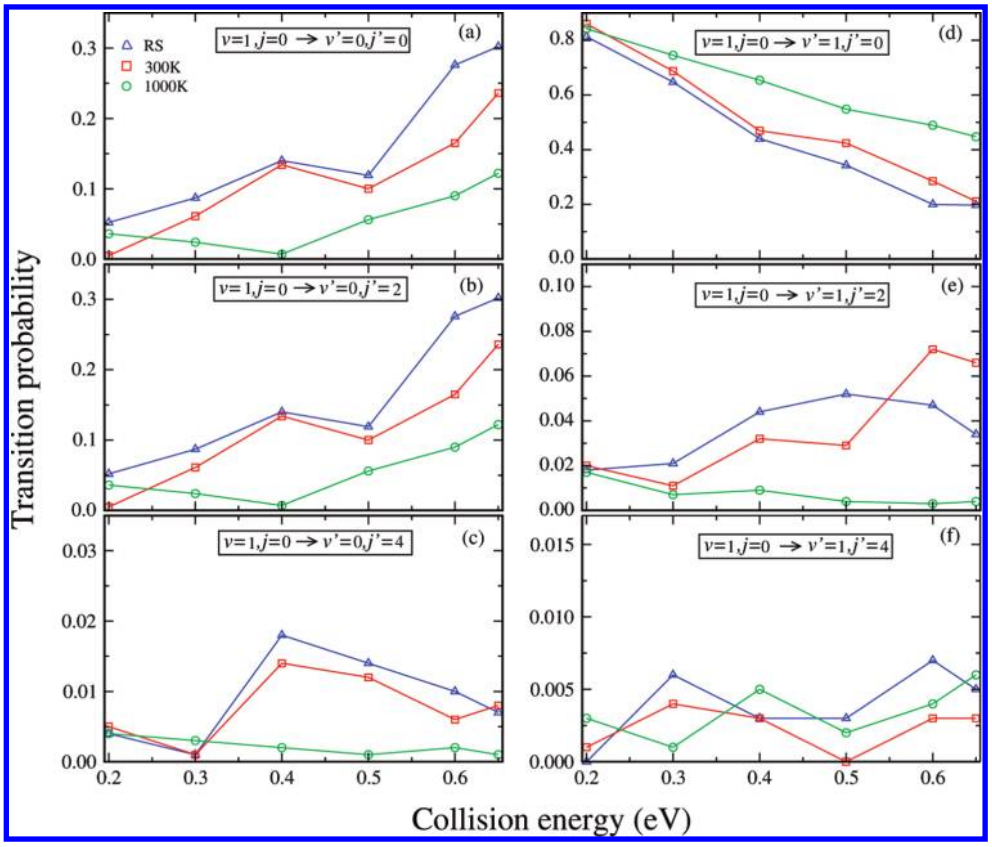

Figure 12. Calculated state-to-state transition probabilities ($v = 1, j = 0 \rightarrow v', j'$) for H_2 on the Cu(100) surface [(a) $v' = 0, j' = 0$; (b) $v' = 0, j' = 2$; (c) $v' = 0, j' = 4$; (d) $v' = 1, j' = 0$; (e) $v' = 1, j' = 2$; (f) $v' = 1, j' = 4$] for RS and two different surface temperatures (300 and 1000 K) included through the BEP factor.

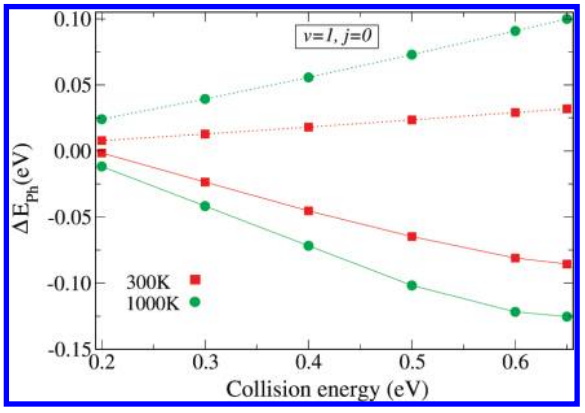

Figure 13. At 300 and 1000 K for the $H_2(v{=}1,j{=}0)-Cu(100)$ system, the energy transfer (ΔE_{Ph}) at asymptotic time within the harmonic approximation (dotted line) and the "exact" energy transfer (solid line) calculated by exploiting the detailed balance eq 16 as a function of initial kinetic energy are presented in the upper and lower part, respectively. The effective Hamiltonian has been formulated by using the BEP factor.

can be considered reasonably accurate to mimic the diatom–surface interaction processes. Such transition probabilities depict little temperature dependence because at sufficiently low initial kinetic energy of the incoming diatom, the overall energy transfer from molecule to the surface is negligibly small.

When we perform 6D quantum dynamics (to treat all molecular DOFs in fully correlated manner) on an effective Hamiltonian (where such Hamiltonian is derived by using BEP factor for initial state distribution of the phonon modes), the calculated sticking probabilities (for the collision $H_2(v{=}0,j{=}0)-Cu(100)$ over the initial KE between 0.3 and 0.9 eV and $H_2(v{=}1,j{=}0)-Cu(100)$ for initial translational energies between 0.2 and 0.65 eV) appear noticeably temperature-dependent, and the corresponding transition probabilities show substantial changes over the temperature range from 300 to 1000 K. In a similar calculation with BEP based Hamiltonian for the $D_2(v{=}0,j{=}0)-Cu(111)$ system, the 6D calculated reaction probabilities have clear temperature dependence and the 4D⊗2D results have noticeable change over the temperature range from 120 to 1000 K. On the contrary, when we formulate an effective Hamiltonian by using BP factor for the initial state distribution of the phonon modes and perform either 4D⊗2D or 6D quantum dynamics for the collision $H_2(v{=}0,j{=}0)-Cu(100)$ over the initial KE from 0.3 to 0.9 eV, the calculated sticking probabilities could not show up any temperature dependence within the temperature range from 300 to 1000 K.

Whenever there is a good agreement between computed reaction probabilities with experimental results[6] (Figures 7a,b and 11a), the estimated barrier heights appear as accurate enough, and in the other case (Figure 10a), such a barrier is far away from the experimental prediction. The EDIM fit bth barrier height for the $H_2-Cu(100)$ system (0.5 eV) is close enough to the DFT-GGA calculated height[21] (0.48 eV), whereas our EDIM fit bth barrier height for the $D_2-Cu(111)$ system (0.38 eV) is away from the ab initio[37] calculated one (0.63 eV). The disagreement between the computed excitation probabilities (Figure 6b) with experimental results[4] strongly indicates the overestimation of anisotropy in the PES.[39] The inaccurate estimation of anisotropy

dx.doi.org/10.1021/jp201524x |J. Phys. Chem. A 2011, 115, 5256–5273

in the PES arises due to the lack of convergence in the DFT calculation and proper fitting procedure. The discrepancies between experimental and theoretical results could also be due to the inappropriate modeling of the molecule−surface scattering processes by neglecting the effects of phonon modes and electron hole−pair excitation. As predicted,[39] the coupling between molecular rotation and electron hole−pair excitation leads to anisotropic charge distribution in the molecule for its different orientation angle. Indeed, this phenomena needs to be explored by constructing appropriate Hamiltonian. On the other hand, we find that the coupling between the molecular DOFs and the surface modes (phonons) could not affect the excitation probabilities [see Figure 6b] at lower collisional energy and surface temperature, but both excitation and de-excitation probabilities [see Figure 7c, 11b, and 12a,b,c,e] decrease substantially as the surface temperature increases.

The equation (15) for energy transfer is formulated within harmonic approximation, which always underestimates the actual energy transfer from molecule to surface or vice versa (see upper part of Figures 8b, 10c, and 13). On the contrary, the lower part of those figures demonstrates a saturation of energy transfer (calculated by using the detailed balance of energy for incoming and outgoing molecule) at higher collisional energy and temperature. These profiles help to understand the interesting feature of the reaction and transition probabilities as a function of initial KEs.

Because our entire theoretical developments and the corresponding calculated results are based on a single projectile [$H_2(v,j)/D_2(v,j)$] colliding with a metal [Cu(100)/Cu(111)] surface, the so-called equilibrium thermodynamic argument on the energy transfer from molecule to the solid or vice versa may not be valid. Even if it is valid, the highest temperature of the surface, at which we have performed the dynamics, corresponds to much less energy (1000 K ≡ 0.086 eV) than the lowest initial kinetic energy (0.30 eV) of the incoming diatom and, thereby, the expected energy transfer will be from molecule to the solid within the temperature and initial KE range of our investigation. Moreover, because the mass difference between the surface atoms and diatom is huge, the recoil energy is very small and that is reflected in the calculated energy transfer through the annihilation process. At this point, it is important to note that the energy transfer from diatom to solid and solid to diatom is represented by creation and annihilation processes with positive and negative magnitudes, respectively. Figure 9b clearly indicates that energy transfer (within harmonic approximation) through the creation process dominates over annihilation ones for all initial kinetic energies and temperatures of our calculations. Because Figure 6c as well as the upper part of Figures 8b, 10c, and 13 show that the total amount of energy transferred (ΔE_{Ph} $(=\Sigma_k(\Delta E_k^+ + \Delta E_k^-))$ calculated within the harmonic approximation is always positive in magnitude, the transfer is dictated by the creation process and it occurs from the diatom to the solid. If we wish to explore the reverse process, namely, the domination of annihilation over creation, probably, the dynamics need to be performed with the surface at very high temperature and the diatom with sufficiently low initial kinetic energy.

In summary, even if we introduce the mean-field approximation between molecular DOFs and phonon modes to keep the calculation computationally tractable, this first principle based approach could bring the temperature dependence on the calculated sticking and transition probabilities depending upon the amount of energy transfer from the molecule to the surface *only when* the effective Hamiltonian is constructed with the BEP factor based approach and, preferably, all molecular DOFs are treated in fully correlated manner by performing 6D quantum dynamics. The reason behind the success of the Bose−Einstein based approach over the Boltzmann could be, as the temperature changes, the average occupation number of the phonons in a quantum state undergoes a change with the BEP based approach rather than the specific occupation number change in case of Boltzmann. Because the excitation of the phonon mode occurs on the X and Y plane, the treatment of X and Y coordinates with other molecular DOFs (x, y, z, and Z) need to be persuaded in a fully correlated manner (6D quantum dynamics) to capture the effect of phonon modes on the molecular DOFs.

APPENDIX A: "STOCHASTIC" TREATMENT FOR THE FORMULATION OF PHONON ENERGY TRANSFER

The energy transfer from the incoming molecule to the solid or vice versa is given by

$$\Delta E_{Ph} = \sum_k \sum_{n_k} \sum_{n_k^0} p_{n_k^0}(E_{n_k} - E_{n_k^0}) P_{n_k^0 \rightarrow n_k} \tag{A1}$$

where $P_{n_k^0 \rightarrow n_k}$ is the kth mode transition probability from quantum state n_k^0 to n_k of a linearly forced harmonic oscillator (LFHO) and the "stochastic" treatment[69,70] of such a model provides the following form of transition probability in terms of modified Bessel function (I_0):

$$P_{n_k^0 \rightarrow n_k} = \frac{1}{\rho_k} \exp[-(n_k + n_k^0 + 1)/\rho_k] \times I_0\left[\frac{2}{\rho_k}\sqrt{\left(n_k + \frac{1}{2}\right)\left(n_k^0 + \frac{1}{2}\right)}\right] \tag{A2}$$

Within the harmonic approximation, the following energy difference between the two quantum states appears as

$$E_{n_k} - E_{n_k^0} = \hbar\omega_k(n_k - n_k^0) \tag{A3}$$

and the occupation probability, $p_{n_k^0}$, in the n_k^0th state for the kth mode at temperature T_s could be determined either by the Boltzmann [eq 10] or by Bose−Einstein [eq 11] probability factor.

We divide the contribution for phonon excitation ($n_k \geq n_k^0$), $\Delta E_{Ph}^+$and de-excitation ($n_k < n_k^0$), ΔE_{Ph}^-, consider the BP factor for the initial state distribution and substitute eqs 10, A2, and A3 in the eq A1 to obtain

$$\Delta E_{Ph}^+ = \sum_k \hbar\omega_k {\rho_k}^{-1}(1 - z_k) \sum_{n_k} \sum_{n_k^0} z_k^{n_k^0}(n_k - n_k^0) \times \exp[-(n_k + n_k^0 + 1)/\rho_k] \times I_0\left[\frac{2}{\rho_k}\sqrt{\left(n_k + \frac{1}{2}\right)\left(n_k^0 + \frac{1}{2}\right)}\right] \tag{A4}$$

which can be simplified to

$$\Delta E_{Ph}^+ = \sum_k \hbar\omega_k {\rho_k}^{-1}(1 - z_k) \sum_m \sum_{n_k^0} z_k^{n_k^0} m \exp\left(-\frac{m}{\rho_k}\right) \times \exp[-(2n_k^0 + 1)/\rho_k] \times I_0\left[\frac{2}{\rho_k}\sqrt{\left(m + n_k^0 + \frac{1}{2}\right)\left(n_k^0 + \frac{1}{2}\right)}\right] \tag{A5}$$

with $m = n_k - n_k^0$. The double sum in eq A5 can be replaced by a double integral to bring an intermediate result:

$$\Delta E_{\mathrm{Ph}}^{+} = \sum_k \hbar\omega_k {\rho_k}^{-1}(1 - z_k)\int_0^\infty \mathrm{d}m\, m \int_0^\infty \mathrm{d}n_k^0\, z_k^{n_k^0} \times \exp[-(2n_k^0 + 1 + m)/\rho_k] \times I_0\left[\frac{2}{\rho_k}\sqrt{\left(m + n_k^0 + \frac{1}{2}\right)\left(n_k^0 + \frac{1}{2}\right)}\right] \quad \text{(A6)}$$

which turns into the following expression under substitution, $x = n_k^0 + {}^1/_2$:

$$\Delta E_{\mathrm{Ph}}^{+} = \sum_k \hbar\omega_k z_k^{-1/2}{\rho_k}^{-1}(1 - z_k)\int_0^\infty \mathrm{d}m\, m \int_0^\infty \mathrm{d}x\, z_k^x \exp[-(2x + m)/\rho_k] \times I_0\left[\frac{2}{\rho_k}\sqrt{(m + x)x}\right]$$
$$= \sum_k \hbar\omega_k z_k^{-1/2}{\rho_k}^{-1}(1 - z_k)\int_0^\infty \mathrm{d}m\, m \exp\left(-\frac{m}{\rho_k}\right)\int_0^\infty \mathrm{d}x\, z_k^x \exp\left(-\frac{2x}{\rho_k}\right) \times I_0\left[\frac{2}{\rho_k}\sqrt{(m + x)x}\right] \quad \text{(A7)}$$

The last part of the above integral can be calculated using the following standard integral[71]

$$\int_0^\infty \mathrm{d}y \exp(-\alpha y) \times I_0(\beta\sqrt{y^2 + 2\gamma y}) = \frac{1}{\sqrt{\alpha^2 - \beta^2}} \times \exp[\gamma(\alpha - \sqrt{\alpha^2 - \beta^2})] \quad \text{(A8)}$$

as given below

$$\mathrm{A} = \int_0^\infty \mathrm{d}x\, z_k^x \exp\left(-\frac{2x}{\rho_k}\right) \times I_0\left[\frac{2}{\rho_k}\sqrt{(m + x)x}\right]$$
$$= \int_0^\infty \mathrm{d}x \exp\left[-\left(\frac{2}{\rho_k} + \hbar\omega_k\beta\right)x\right] \times I_0\left[\frac{2}{\rho_k}\sqrt{(m + x)x}\right]$$
$$= \frac{1}{\sqrt{a_k^{(1)}}} \exp\left[\frac{m}{2}\left\{\frac{2}{\rho_k} + \hbar\omega_k\beta - \sqrt{a_k^{(1)}}\right\}\right] \quad \text{(A9)}$$

and substituted back to eq A7 to obtain

$$\Delta E_{\mathrm{Ph}}^{+} = \sum_k \hbar\omega_k z_k^{-1/2}{\rho_k}^{-1}\frac{1}{\sqrt{a_k^{(1)}}}(1 - z_k) \times \int_0^\infty \mathrm{d}m\, m \exp\left(-\frac{m}{\rho_k}\right) \exp\left[\frac{m}{2}\left\{\frac{2}{\rho_k} + \hbar\omega_k\beta - \sqrt{a_k^{(1)}}\right\}\right]$$
$$= \sum_k \hbar\omega_k z_k^{-1/2}{\rho_k}^{-1}\frac{1}{\sqrt{a_k^{(1)}}}(1 - z_k) \times \int_0^\infty \mathrm{d}m\, m \exp\left[\frac{m}{2}\{\hbar\omega_k\beta - \sqrt{a_k^{(1)}}\}\right] \quad \text{(A10)}$$

where $a_k^{(1)} = \beta^2\hbar^2{\omega_k}^2 + 4\beta\hbar\omega_k{\rho_k}^{-1}$.

The final form of phonon energy transfer for the kth mode in the creation process after substituting the standard integration[71]

$$\int_0^\infty \mathrm{d}y\, y \times \exp(-ay) = \frac{1}{a^2} \quad \text{(A11)}$$

over m with analytical simplification becomes

$$\Delta E_k^{+} = \frac{4\hbar\omega_k}{\rho_k\sqrt{a_k^{(1)}}}(1 - z_k){z_k}^{-1/2}\left(\beta\hbar\omega_k - \sqrt{a_k^{(1)}}\right)^{-2} \quad \text{(A12a)}$$

and, similarly, the expression for annihilation processes appears,

$$\Delta E_k^{-} = -\frac{4\hbar\omega_k}{\rho_k\sqrt{a_k^{(1)}}}(1 - z_k){z_k}^{-1/2}\left(\beta\hbar\omega_k + \sqrt{a_k^{(1)}}\right)^{-2} \quad \text{(A12b)}$$

Therefore, we find the total energy transferred from the incoming molecule to phonon modes or vice versa as

$$\Delta E_{\mathrm{Ph}} = \Delta E_{\mathrm{Ph}}^{+} + \Delta E_{\mathrm{Ph}}^{-} = \sum_k \hbar\omega_k\rho_k\frac{\sinh(\Delta_k)}{\Delta_k} \quad \text{(A13)}$$

where $\Delta_k = {}^1/_2\hbar\omega_k\beta$. It is quite important to note that energy transfer due to the initial state distribution of the phonon nodes with the BP factor appears to be surface temperature-independent.

When we consider the BEP factor for the initial state distribution and substitute eqs 11, A2, and A3 into eq A1, the expression of energy transfer for creation processes appears as

$$\Delta E_{\mathrm{Ph}}^{+} = \sum_k \hbar\omega_k{\rho_k}^{-1}\sum_{n_k}\sum_{n_k^0}(n_k - n_k^0)(z_k^{n_k^0} + z_k^{2n_k^0} + z_k^{3n_k^0} + z_k^{4n_k^0} + \ldots) \times \exp[-(n_k + n_k^0 + 1)/\rho_k] \times I_0\left[\frac{2}{\rho_k}\sqrt{\left(n_k + \frac{1}{2}\right)\left(n_k^0 + \frac{1}{2}\right)}\right] \quad \text{(A14)}$$

which can be simplified to

$$\Delta E_{\mathrm{Ph}}^{+} = \sum_k \hbar\omega_k{\rho_k}^{-1}\sum_m m \exp\left(-\frac{m}{\rho_k}\right)\sum_{n_k^0}(z_k^{n_k^0} + z_k^{2n_k^0} + z_k^{3n_k^0} + z_k^{4n_k^0} + \ldots) \times \exp[-(2n_k^0 + 1)/\rho_k] I_0\left[\frac{2}{\rho_k}\sqrt{\left(m + n_k^0 + \frac{1}{2}\right)\left(n_k^0 + \frac{1}{2}\right)}\right] \quad \text{(A15)}$$

with $m = n_k - n_k^0$. The double sum in eq A15 can be replaced by a double integral to obtain an intermediate result:

$$\Delta E_{\mathrm{Ph}}^{+} = \sum_k \hbar\omega_k{\rho_k}^{-1}\int_0^\infty \mathrm{d}m\, m \exp\left(-\frac{m}{\rho_k}\right) \int_0^\infty \mathrm{d}n_k^0\, (z_k^{n_k^0} + z_k^{2n_k^0} + z_k^{3n_k^0} + z_k^{4n_k^0} + \ldots) \times \exp[-(2n_k^0 + 1)/\rho_k] \times I_0\left[\frac{2}{\rho_k}\sqrt{\left(m + n_k^0 + \frac{1}{2}\right)\left(n_k^0 + \frac{1}{2}\right)}\right] \quad \text{(A16)}$$

which turns into the following expression under substitution, $x = n_k^0 + {}^1/_2$:

$$\Delta E_{\mathrm{Ph}}^{+} = \sum_k \hbar\omega_k{\rho_k}^{-1}\int_0^\infty \mathrm{d}m\, m \exp\left(-\frac{m}{\rho_k}\right) \times \int_0^\infty \mathrm{d}x\, (z_k^{x - 1/2} + z_k^{2x - 1} + z_k^{3x - 3/2} + z_k^{4x - 2} + \ldots) \times \exp\left[-\frac{2x}{\rho_k}\right] \times I_0\left[\frac{2}{\rho_k}\sqrt{(m + x)x}\right] \quad \text{(A17)}$$

dx.doi.org/10.1021/jp201524x | J. Phys. Chem. A 2011, 115, 5256–5273

The above standard integrals,[71] eqs A8 and A11, are substituted in eq A17, integrated over x and m and simplified analytically to obtain the final form of energy transfer for kth mode in the creation process as

$$\Delta E_k^{+} = \hbar\omega_k \rho_k^{-1} \sum_{n=1}^{\infty} 4a_k^{(n)^{-1/2}} z_k^{-n/2} \left[n\hbar\omega_k\beta - \sqrt{a_k^{(n)}} \right]^{-2} \tag{A18a}$$

and, similarly, the expression for annihilation processes appears,

$$\Delta E_k^{-} = -\hbar\omega_k \rho_k^{-1} \sum_{n=1}^{\infty} 4a_k^{(n)^{-1/2}} z_k^{-n/2} \left[n\hbar\omega_k\beta + \sqrt{a_k^{(n)}} \right]^{-2} \tag{A18b}$$

where

$$a_k^{(n)} = n^2\beta^2\hbar^2\omega_k^{\,2} + 4n\beta\hbar\omega_k\rho_k^{-1} \tag{A19}$$

Thus, the total energy transfer from molecule to the solid or vice versa is expressed as

$$\Delta E_{\mathrm{Ph}} = \Delta E_{\mathrm{Ph}}^{+} + \Delta E_{\mathrm{Ph}}^{-} = \sum_k k_{\mathrm{B}} T_{\mathrm{s}} \rho_k \sum_{n=1}^{\infty} \frac{x_k^n}{n} \tag{A20}$$

where $x_k = \exp(^1/_2\hbar\omega_k\beta)$.

Thus, the energy transfer due to the inclusion of the BEP factor for the initial state distribution of the phonon modes brings the surface temperature dependence.

APPENDIX B: EXPLICIT FORM OF THE MATRICES USED IN THE TDDVR QUANTUM AND CLASSICAL EQUATIONS OF MOTION

The explicit forms of the matrices used in the quantum-classical equation of motion are presented as follows:

$$\bar{G}_{i_k,i'_k} = \frac{G_{i_k,i'_k}}{\sqrt{A_{i_k,i_k}A_{i'_k,i'_k}}} \qquad \bar{F}_{i_k,i'_k} = \frac{F_{i_k,i'_k}}{\sqrt{A_{i_k,i_k}A_{i'_k,i'_k}}}$$

$$d_{i_1 i_2 \ldots i_p} = c_{i_1 i_2 \ldots i_p} \prod_{k=1}^{p} (A_{i_k,i_k})^{1/2} \qquad A_{i_k,i'_k} = \sum_{n=0}^{N_k} \xi_n^*(x_{i_k})\, \xi_n(x_{i'_k})$$

$$G_{i_k,i'_k} = \sum_{n=0}^{N_k-1} \xi_{n+1}^*(x_{i_k})\sqrt{n+1}\,\xi_n(x_{i'_k}) + \sum_{n=1}^{N_k} \xi_{n-1}^*(x_{i_k})\sqrt{n}\,\xi_n(x_{i'_k})$$

$$F_{i_k,i'_k} = \sum_{n=0}^{N_k-2} \xi_{n+2}^*(x_{i_k})\sqrt{(n+1)(n+2)}\,\xi_n(x_{i'_k}) + \sum_{n=2}^{N_k} \xi_{n-2}^*(x_{i_k})\sqrt{n(n-1)}\,\xi_n(x_{i'_k}) - \sum_{n=0}^{N_k} \xi_n^*(x_{i_k})(2n-1)\xi_n(x_{i'_k}) \tag{B1}$$

The TDDVR equation of motion for the quantum dynamics has the following important characteristics: (a) The component matrices ($\{A_k\}$, $\{G_k\}$, $\{F_k\}$) of the TDDVR Hamiltonian matrix [see eq 27] are time-independent and need to be evaluated once and for all. (b) Because the matrices, $\{G_k\}$, are diagonal and associated with the "classical" variables $\{P_{X_k}(t)\}$,thenonlineardynamicsofthese"classical"quantities affects the convergence but not the final solution of the quantum equations of motion. (c) As the off-diagonal propagation of their associated parameters, $\{\mathrm{Im}\, A_k\}$, is not desirable, hence, a time-independent $\{\mathrm{Im}\, A_k\}$ is the obvious choice.

The explicit form of R, $S^{(n)}$, and T matrices involved in the "classical" equation of motion are

$$R_{i_k i'_k} = \sum_p \xi_p^*(x_{i_k})\, \xi_p(x_{i'_k}) 2p$$

$$S^{(n)}_{i_k i'_k} = \sum_{pq} \xi_p^*(x_{i_k})\, \xi_q(x_{i'_k}) \int \Phi_q^*(X_k,t)(X_k - X_k^c(t))^n \Phi_p(X_k,t)\, \mathrm{d}X_k$$

$$T_{i_k i'_k} = \sum_{pq} \xi_p(x_{i_k})\, \xi_q^*(x_{i'_k}) 2p \int \Phi_p^*(X_k,t)(X_k - X_k^c(t))\Phi_q(X_k,t)\, \mathrm{d}X_k \tag{B2}$$

with

$$\int \Phi_p^*(X_k,t)(X_k - X_k^c(t))\Phi_q(X_k,t)\, \mathrm{d}X_k = \frac{1}{2}\sqrt{\frac{\hbar}{\mathrm{Im}\, A_k}} \left\{ \sqrt{p+1}\,\delta_{p+1,q} + \sqrt{p}\,\delta_{p-1,q} \right\}$$

$$\int \Phi_p^*(X_k,t)(X_k - X_k^c(t))\Phi_q(X_k,t)\, \mathrm{d}X_k = \frac{\hbar}{4\,\mathrm{Im}\, A_k} \left\{ \sqrt{(p+1)(p+2)}\,\delta_{p+2,q} + (2p+1)\delta_{p,q} + \sqrt{p(p-1)}\,\delta_{p-2,q} \right\}$$

$$\int \Phi_p^*(X_k,t)(X_k - X_k^c(t))^3 \Phi_q(X_k,t)\, \mathrm{d}X_k = \frac{1}{8}\left(\frac{\hbar}{\mathrm{Im}\, A_k}\right)^{3/2} \times \left\{ \sqrt{(p+1)(p+2)(p+3)}\,\delta_{p+3,q} + 3(p+1)\sqrt{p+1}\,\delta_{p+1,q} + 3p\sqrt{p}\,\delta_{p-1,q} + \sqrt{p(p-1)(p-2)}\,\delta_{p-3,q} \right\} \tag{B3}$$

AUTHOR INFORMATION

Corresponding Author

*Fax: +91-33-2473 2805. E-mail: pcsa@iacs.res.in.

ACKNOWLEDGMENT

T.S. and S.S. acknowledge CSIR, India, for research fellowship and SA acknowledges DST, India, through project no. SR/S1/PC-13/2008 for the research funding.

REFERENCES

(1) Rettner, C. T.; Ashfold, M. N. R. *Dynamics of Gas - Surface Interactions*; Royal Society of Chemistry: London, 1991.
(2) Balooch, M.; Stickney, R. E. *Surf. Sci.* **1974**, *44*, 310.
(3) Anger, G.; Winkler, A; Rendulic, K. D. *Surf. Sci.* **1989**, *220*, 1.
(4) Watts, E.; Sitz, G. O. *J. Chem. Phys.* **2001**, *114*, 4171.
(5) Rendulic, K. D.; Winkler, A. *Surf. Sci.* **1994**, *299/300*, 261.
(6) Michelsen, H. A.; Auerbach, D. J. *J. Chem. Phys.* **1991**, *94*, 7502.
(7) Michelsen, H. A.; Rettner, C. T.; Auerbach, D. J. *Surf. Sci.* **1992**, *272*, 65.
(8) Rettner, C. T.; Michelsen, H. A.; Auerbach, D. J. *Faraday Discuss.* **1993**, *96*, 17.
(9) Rettner, C. T.; Auerbach, D. J.; Michelsen, H. A. *Phys. Rev. Lett.* **1992**, *68*, 1164.

(10) Cacciatore, M.; Billing, G. D. *Surf. Sci.* **1990**, *232*, 35.
(11) Darling, D. R.; Holloway, S. *Rep. Prog. Phys.* **1995**, *58*, 1595.
(12) Mowrey, R. C.; Kroes, G. J.; Baerends, E. J. *J. Chem. Phys.* **1998**, *108*, 6906.
(13) McCormack, D. A.; Kroes, G. J.; Olsen, R. A.; Baerends, E. J.; Mowrey, R. C. *Phys. Rev. Lett.* **1999**, *82*, 1410.
(14) Baer, M. *J. Chem. Phys.* **1984**, *81*, 4526.
(15) Baer, M. *Chem. Phys. Lett.* **1985**, *116*, 439.
(16) Shima, Y.; Baer, M. *J. Chem. Phys.* **1985**, *83*, 5250.
(17) Hammer, B.; Scheffler, M.; Jacobsen, K. W.; Nørskov, J. K. *Phys. Rev. Lett.* **1994**, *73*, 1400.
(18) White, J. A.; Bird, D. M. *Chem. Phys. Lett.* **1993**, *213*, 422.
(19) Madhavan, P.; Whitten, J. L. *J. Chem. Phys.* **1982**, *77*, 2673.
(20) White, J. A.; Bird, D. M.; Payne, M. C.; Stich, I. *Phys. Rev. Lett.* **1994**, *73*, 1404.
(21) Wiesenekker, G.; Kroes, G. J.; Baerends, E. J. *J. Chem. Phys.* **1996**, *104*, 7344.
(22) Kratzer, P.; Hammer, B.; Nørskov, J. K. *Surf. Sci.* **1996**, *359*, 45.
(23) Truong, T. N.; Truhlar, D. G.; Garrett, B. C. *J. Phys. Chem.* **1989**, *93*, 8227.
(24) Billing, G. D. *J. Phys. Chem.* **1995**, *99*, 15378.
(25) Kosloff, D.; Kosloff, R. *J. Comput. Phys.* **1983**, *52*, 35.
(26) Kosloff, R. *J. Phys. Chem.* **1988**, *92*, 2087.
(27) Ehara, M.; Meyer, H.-D.; Cederbaum, L. S. *J. Chem. Phys.* **1996**, *105*, 8865.
(28) Wang, Z. S.; Darling, D. R.; Holloway, S. *Phys. Rev. Lett.* **2001**, *87*, 226102.
(29) Nave, S.; Jackson, B. *Phys. Rev. Lett.* **2007**, *98*, 173003.
(30) Tiwari, A. K.; Nave, S.; Jackson, B. *Phys. Rev. Lett.* **2009**, *103*, 253201.
(31) Tiwari, A. K.; Nave, S.; Jackson, B. *J. Chem. Phys.* **2010**, *132*, 134702.
(32) Billing, G. D. *J. Phys. Chem. A* **2001**, *105*, 2340.
(33) Billing, G. D. *Phys. Chem. Chem. Phys.* **2002**, *4*, 2865.
(34) Gross, A.; Wilke, S.; Scheffler, M. *Phys. Rev. Lett.* **1995**, *75*, 2718.
(35) Dai, J.; Light, J. C. *J. Chem. Phys.* **1997**, *107*, 1676.
(36) Kroes, G. J.; Baerends, E. J.; Mowrey, R. C. *Phys. Rev. Lett.* **1997**, *78*, 3583.
(37) Díaz, C.; Pijper, E.; Olsen, R. A.; Busnengo, H. F.; Auerbach, D. J.; Kroes, G. J. *Science* **2009**, *326*, 832.
(38) Kroes, G. J.; Baerends, E. J.; Mowrey, R. C. *J. Chem. Phys.* **1997**, *107*, 3309.
(39) Watts, E.; Sitz, G. O.; McCormack, D. A.; Kroes, G. J.; Olsen, R. A.; Groeneveld, J. A.; Stralen, J. N. P.; Van; Baerends, E. J.; Mowrey, R. C. *J. Chem. Phys.* **2001**, *114*, 495.
(40) Mowrey, R. C.; McCormack, D. A.; Kroes, G. J.; Baerends, E. J. *J. Chem. Phys.* **2001**, *114*, 7581.
(41) Gross, A.; Hammer, B.; Scheffler, M.; Brenig, W. *Phys. Rev. Lett.* **1994**, *73*, 3121.
(42) Nave, S.; Lemoine, D.; Somers, M. F.; Kingma, S. M.; Kroes, G. J. *J. Chem. Phys.* **2005**, *122*, 214709.
(43) Kroes, G. J.; Pijper, E.; Salin, A. *J. Chem. Phys.* **2007**, *127*, 164722.
(44) Hand, M.; Harris, J. *J. Chem. Phys.* **1990**, *92*, 7610.
(45) Luntz, A. C.; Harris, J. *Surf. Sci.* **1991**, *258*, 397.
(46) Dohle, M.; Saalfrank, P. *Surf. Sci.* **1997**, *373*, 95.
(47) Billing, G. D. *Chem. Phys.* **1982**, *70*, 223.
(48) Billing, G. D. *Dynamics of molecule surface Interactions*; John Wiley & Sons: New York, 2000.
(49) Adhikari, S.; Billing, G. D. *J. Chem. Phys.* **2000**, *112*, 3884.
(50) Sahoo, T.; Sardar, S.; Adhikari, S. *Phys. Chem. Chem. Phys.* **2011**, DOI: 10.1039/c0cp00336k.
(51) Perdew, J. P.; Chevary, J. A.; Vosko, S. H.; Jackson, K. A.; Pederson, M. R.; Singh, D. J.; Fiolhais, C. *Phys. Rev. B* **1992**, *46*, 6671.
(52) Becke, A. D. *Phys. Rev. A* **1988**, *38*, 3098.
(53) Perdew, J. P. *Phys. Rev. B* **1986**, *33*, 8822.
(54) Pechukas, P.; Light, J. C. *J. Chem. Phys.* **1966**, *44*, 3897.
(55) Billing, G. D.; Adhikari, S. *Chem. Phys. Lett.* **2000**, *321*, 197.
(56) Adhikari, S.; Billing, G. D. *J. Chem. Phys.* **2000**, *113*, 1409.
(57) Barkakaty, B.; Adhikari, S. *J. Chem. Phys.* **2003**, *118*, 5302.
(58) Puzari, P.; Sarkar, B.; Adhikari, S. *J. Chem. Phys.* **2004**, *121*, 707.
(59) Puzari, P.; Sarkar, B.; Adhikari, S. *Int. J. Quantum Chem.* **2005**, *105*, 209.
(60) Puzari, P.; Swathi, R. S.; Sarkar, B.; Adhikari, S. *J. Chem. Phys.* **2005**, *123*, 134317.
(61) Puzari, P.; Sarkar, B.; Adhikari, S. *J. Chem. Phys.* **2006**, *125*, 194316.
(62) Sardar, S.; Paul, A. K.; Mondal, P.; Sarkar, B.; Adhikari, S. *Phys. Chem. Chem. Phys.* **2008**, *10*, 6388.
(63) Sardar, S.; Paul, A. K.; Sharma, R.; Adhikari, S. *J. Chem. Phys.* **2009**, *130*, 144302.
(64) Sardar, S.; Paul, A. K.; Adhikari, S. *Mol. Phys.* **2009**, *107*, 2467.
(65) Sardar, S.; Paul, A. K.; Sharma, R.; Adhikari, S. *Int. J. Quantum Chem.*, DOI:10.1002/qua.22578.
(66) Sardar, S.; Puzari, P.; Adhikari, S. *Chem. Phys. Lett.* **2010**, *496*, 341.
(67) Dirac, P. A. M. *Proc. Cambridge Philos. Soc.* **1930**, *26*, 376.
(68) Cullum, J. K.; Willoughby, R. A. *Lanczos Algorithms for Large Symmetric Eigenvalue Computations*; Birkhauser: Boston, 1985.
(69) Schatz, G. C.; McLafferty, F. J.; Ross, J. *J. Chem. Phys.* **1977**, *66*, 3609.
(70) Billing, G. D.; Eu, B. C.; Nyeland, C. *Chem. Phys.* **1978**, *29*, 427.
(71) Gradshteyn, I. S.; Ryzhik, J. M. *Table of integrals, series and products*; Academic Press: New York, 1965.